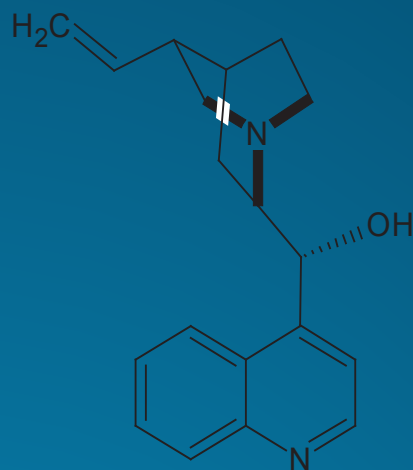
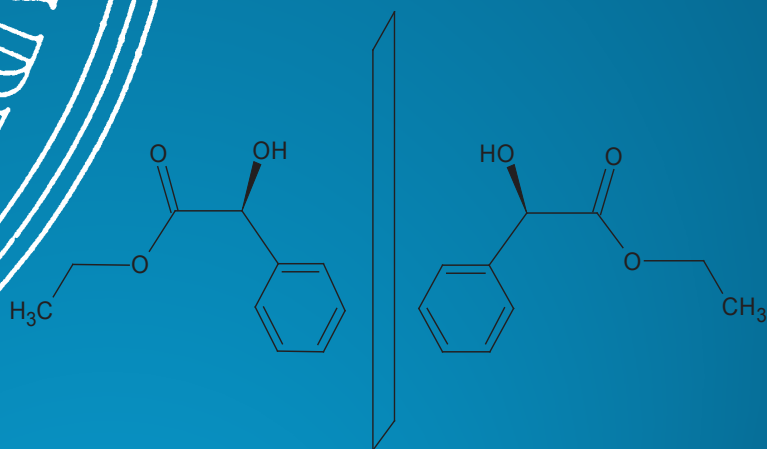


# Novel technology for preparation of optically active chemicals



Gerson E. Martin Curvelo



Laboratory of Industrial Chemistry and Reaction Engineering  
Process Chemistry Centre  
Department of Chemical Engineering  
Åbo Akademi University  
Turku/Åbo 2014

# Novel technology for preparation of optically active chemicals

**Gerson E. Martin Curvelo**



Laboratory of Industrial Chemistry and Reaction Engineering

Process Chemistry Centre

Department of Chemical Engineering

Åbo Akademi University

Turku/Åbo 2014

*Supervised by*

Academy Professor Tapio Salmi  
Laboratory of Industrial Chemistry and Reaction Engineering  
Åbo Akademi University, Finland

Professor Dmitry Yu. Murzin  
Laboratory of Industrial Chemistry and Reaction Engineering  
Åbo Akademi University, Finland

*Co-supervised by*

Professor Henrik Saxén  
Laboratory of Thermal and Flow Engineering  
Åbo Akademi University, Finland

Professor Frank Pettersson  
Laboratory of Process Design and Systems Engineering  
Åbo Akademi University, Finland

*Reviewers*

Doc. Dr. Esa Toukoniitty  
Helsinki Metropolia University of Applied Science, Finland

Prof. Dr. Dr. habil. Andreas Seidel-Morgenstern  
Otto-von-Guericke Universität Magdeburg

*Opponent*

Doc. Dr. Esa Toukoniitty  
Helsinki Metropolia University of Applied Science, Finland

ISBN 978-952-12-3072-1  
Painosalama Oy – Turku/Åbo, Finland 2014

*A quien pueda interesar*

## **PREFACE**

The present work was carried out at the Laboratory of Industrial Chemistry and Reaction Engineering, Department of Chemical Engineering at Åbo Akademi University between 2010 and 2013. The research is part of the activities at Åbo Akademi Process Chemistry Centre (PCC), a centre of excellence financed by Åbo Akademi University. Financial support from the Academy of Finland is gratefully acknowledged.

I would like to express my gratitude to Professor Tapio Salmi for his enthusiasm and great ideas during this project, to Professor Dmitry Yu. Murzin for his valuable scientific contribution and shared experience, to Docent Päivi Mäki-Arvela for her energetic participation and to Lab. Manager Dr Kari Eränen for his invaluable collaboration and help during all these years. I would like also to acknowledge Docent Johan Wärnå for sharing his knowledge in kinetic modeling. Special thanks go to Professors Henrik Saxén and Frank Pettersson for their support during our more than, 25 project meetings.

I would like to thank all the co-authors and co-workers from Åbo Akademi University (Finland), Jyväskylä University (Finland) and Porto University (Portugal) for fruitful and successful collaboration. I hope that our cooperation will continue in the future.

My friends have contributed to make this possible. I would like to thank to Alexey Kirilin, Bartosz Rozmysłowicz, Cesar Araujo, Ekaterina Korotkova, Sabrina Schmidt, Victor Sifontes, Claudio Carletti, Lotta Österholm and many more for their support and understanding throughout the recent years.

I would like to thank my family and specially my mother for her patience and understanding and last but not least to my girlfriend Heidi for her unconditional love, kiitos.

Turku/Åbo, March 15<sup>th</sup>, 2014

Gerson Martin

## ABSTRACT

Gerson E. Martin Curvelo

### **Novel technology for preparation of optically active chemicals: enantioselective hydrogenation coupled to chromatographic separation**

Keywords: Enantioselective hydrogenation, modified Pt catalyst, catalyst deactivation, solvent effect, transition state theory, dielectric constant, kinetic model, multi-centered adsorption, continuous operation, adsorption isotherm, chromatographic separation.

Asymmetric synthesis using modified heterogeneous catalysts has gained lots of interest in the production of optically pure chemicals, such as pharmaceuticals, nutraceuticals, fragrances and agrochemicals. Heterogeneous modified catalysts capable of inducing high enantioselectivities are preferred in industrial scale due to their superior separation and handling properties. The topic has been intensively investigated both in industry and academia.

The enantioselective hydrogenation of ethyl benzoylformate (EBF) to (*R*)-ethyl mandelate over (-)-cinchonidine (CD)-modified Pt/Al<sub>2</sub>O<sub>3</sub> catalyst in a laboratory-scale semi-batch reactor was studied as a function of modifier concentration, reaction temperature, stirring rate and catalyst particle size. The main product was always (*R*)-ethyl mandelate while small amounts of (*S*)-ethyl mandelate were obtained as by product. The kinetic results showed higher enantioselectivity and lower initial rates approaching asymptotically to a constant value as the amount of modifier was increased. Additionally, catalyst deactivation due to presence of impurities in the feed was prominent in some cases; therefore activated carbon was used as a cleaning agent of the raw material to remove impurities prior to catalyst addition. Detailed characterizations methods (SEM, EDX, TPR, BET, chemisorption, particle size distribution) of the catalysts were carried out.

Solvent effects were also studied in the semi-batch reactor. Solvents with dielectric constant ( $\epsilon$ ) between 2 and 25 were applied. The enantiomeric excess (ee) increased with an increase of the dielectric coefficient up to a maximum followed by a nonlinear decrease. A kinetic model was proposed for the enantioselectivity dependence on the dielectric constant

based on the Kirkwood treatment. The non-linear dependence of  $ee$  on  $(\epsilon)$  successfully described the variation of  $ee$  in different solvents.

Systematic kinetic experiments were carried out in the semi-batch reactor. Toluene was used as a solvent. Based on these results, a kinetic model based on the assumption of different number of sites was developed. Density functional theory calculations were applied to study the energetics of the EBF adsorption on pure Pt(1 1 1). The hydrogenation rate constants were determined along with the adsorption parameters by non-linear regression analysis. A comparison between the model and the experimental data revealed a very good correspondence.

Transient experiments in a fixed-bed reactor were also carried out in this work. The results demonstrated that continuous enantioselective hydrogenation of EBF in hexane/2-propanol 90/10 (v/v) is possible and that continuous feeding of (-)-cinchonidine is needed to maintain a high steady-state enantioselectivity. The catalyst showed a good stability and high enantioselectivity was achieved in the fixed-bed reactor.

Chromatographic separation of (*R*)- and (*S*)-ethyl mandelate originating from the continuous reactor was investigated. A commercial column filled with a chiral resin was chosen as a perspective preparative-scale adsorbent. Since the adsorption equilibrium isotherms were linear within the entire investigated range of concentrations, they were determined by pulse experiments for the isomers present in a post-reaction mixture. Breakthrough curves were measured and described successfully by the dispersive plug flow model with a linear driving force approximation.

The focus of this research project was the development of a new integrated production concept of optically active chemicals by combining heterogeneous catalysis and chromatographic separation technology. The proposed work is fundamental research in advanced process technology aiming to improve efficiency and enable clean and environmentally benign production of enantiomeric pure chemicals.

## REFERAT

Gerson E. Martin Curvelo

### **Ny teknologi för preparering av optiskt aktiva kemikalier: enantioselektiv hydrering kopplad till kromatografisk separering**

Nyckelord: enantioselektiv hydrering, modifierad platinakatalysator, katalysatordeaktivering, lösningsmedeleffekt, övergångstillståndsteori, dielektricitetskonstant, kinetisk modell, adsorption på flera centra, kontinuerlig drift, adsorptionsisoterm, kromatografisk separering

Asymmetrisk syntes med hjälp av modifierade heterogena katalysatorer har fått mycket uppmärksamhet i produktion av optiskt rena kemikalier, såsom farmaceutiska produkter, tillsatsämnen i livsmedel, luktämnen samt jordbrukskemikalier. Heterogena modifierade katalysatorer som kan inducera höga enantioselektiviteter prefereras i industriell skala p.g.a. att de kan hanteras bekvämt och separeras lätt från reaktionsvätskor. Detta tema har forskats intensivt både av industrin och det akademiska samfundet.

Enantioselektiv hydrering av etylbensoylformat (EBF) till (*R*)-etylmandelat på (-)-cinkoninidmodifierad (CD) platina-aluminiumoxidkatalysator studerades i en halvkontinuerlig reaktor i laboratorieskala. Modifierarkoncentration, reaktionstemperatur, omrörarhastighet och katalysatorpartikelstorlek var de viktigaste reaktionsparametrarna. Huvudprodukten var alltid (*R*)-etylmandelat, medan små mängder av (*S*)-etylmandelat erhöles som biprodukt. Kinetiska resultat visade stigande enantioselektiviteter och avtagande begynnelsehastigheter, vilka närmade sig asymptotiska värden då modifierarmängden ökades. Katalysatordeaktivering förorsakad av orenheter i råvaran var förödande i vissa fall. Därför användes aktivt kol som rengörande adsorbent för råvaran innan katalysatorn tillsattes systemet. Katalysatorerna karakteriserades grundligt med flera metoder (SEM, EDX, TPR, BET, kemisorption, partikelstorleksfördelning).

Lösningsmedeleffekter studerades i experiment vilka genomfördes i den halvkontinuerliga reaktorn. Lösningemedel som hade dielektricitetskonstanter ( $\epsilon$ ) mellan 2 och 25 användes i dessa experiment. Det enantiomera överskottet (*ee*) ökade med ökande dielektricitetskonstant tills ett maximum uppnåddes, varefter överskottet minskade olinjärt.

En kinetisk modell föreslogs för enantioselektivitetens beroende av dielektricitetskonstanten. Modellen baserade sig på Kirkwoods teori. Det olinjära sambandet mellan enantioselektivitet och dielektricitetskonstant beskrev framgångsrikt enantioselektivitetens variationer i olika lösningsmedel.

Systematiska kinetiska experiment genomfördes i den halvkontinuerliga reaktorn. Toluén användes som lösningsmedel. På basis av dessa resultat utvecklades en kinetisk modell som grundar sig på hypotesen för olika antal adsorptionssäten för olika molekyler och molekylformer. Teoretiska beräkningar som baserade sig på densitetsfunktionalitetsteorin (DFT) användes för att studera EBF:s adsorption på rena Pt(111)-ytor. Hastighetskonstanter och adsorptionsparametrar för hydreringsprocessen bestämdes med hjälp av icke-linjär regressionsanalys. En jämförelse mellan experimentella data och modellens prediktioner avslöjade en mycket god överensstämmelse.

Även transienta experiment i en packad bäddreaktor genomfördes i detta arbete. Resultaten visade att kontinuerlig enantioselektiv hydrering av EBF i en blandning av hexan och 2-propanol (90:10 i viktprocent) var möjlig, men det är nödvändigt att kontinuerligt tillföra (-)-cinkonidin för att upprätthålla en hög enantioselektivitet i fortfarighetstillståndet. Katalysatorn visade en god stabilitet och en hög enantioselektivitet i bäddreaktorn.

Kromatografisk separering av (*R*)- och (*S*)-etylmandelat som härstammade från den kontinuerliga bäddreaktorn studerades ingående. En kommersiell kolonn fylld med en kiral harts valdes som ett möjligt adsorptionssystem i preparativ skala. Eftersom komponenternas adsorptionsisotermer var linjära inom det studerade koncentrationsområdet, kunde de bestämmas med pulsexperiment för isomerer i reaktionsblandningen som härstammade från bäddreaktorn. Genombrottskurvor uppmättes och beskrevs med framgång med dispersiv kolvströmningsmodell och linjär drivkraftsapproximation.

Tyngdpunkten i detta forskningsprojekt var utvecklingen av ett nytt, integrerat produktionskoncept för optiskt aktiva kemikalier genom att kombinera heterogen katalys och kromatografisk separationsteknologi. Arbetet representerar grundforskning i avancerad processteknologi med målsättningen att förbättra processens effektivitet och möjliggöra en miljövänlig produktion av optiskt rena kemikalier.

## RESUMEN

Gerson E. Martin Curvelo

### **Nueva tecnología para la preparación de químicos ópticamente activos: hidrogenación enantioselectiva acoplada con separación cromatográfica.**

Palabras clave: Hidrogenación enantioselectiva, catalizador de Pt modificado, desactivación del catalizador, efecto del solvente, teoría del estado de transición, constante dieléctrica, modelo cinético, adsorción multicentrada, operación continua, isothermas de adsorción, separación cromatográfica.

La síntesis asimétrica usando catalizadores heterogéneos modificados ha obtenido un gran interés en la producción de compuestos ópticamente puros, tales como: fármacos, nutracéuticos, fragancias y agroquímicos. Los catalizadores heterogéneos modificados capaces de inducir altas enantioselectividades son preferidos a escala industrial por sus propiedades de fácil manejo y separación. Este tema ha sido investigado intensivamente tanto en la industria como en la academia.

La hidrogenación enantioselectiva de etil formato de benzoilo (EBF, por sus siglas en inglés) hacia (*R*)-mandelato de etilo sobre (-)-cinchonidin (CD) Pt/Al<sub>2</sub>O<sub>3</sub> modificado en un reactor semi-batch a escala de laboratorio fue estudiado en función de la concentración del modificador, temperatura, velocidad de agitación y el tamaño de partícula del catalizador. El principal producto fue siempre (*R*)-mandelato de etilo mientras que pequeñas cantidades de (*S*)-mandelato de etilo fueron obtenidas como producto secundario. Los resultados cinéticos mostraron altas enantioselectividades y bajas velocidades iniciales que se acercaban a valores asintóticos a medida que la cantidad de modificador se incrementaba. Adicionalmente, la desactivación del catalizador debido a la presencia de impurezas en la alimentación fue prominente en algunos casos; es por ello que se usó carbón activado como un agente purificador de la materia prima a fin de remover dichas impurezas y evitar así el contacto con el catalizador. Distintos métodos de caracterización (SEM, EDX, TPR, BET, quimisorción, distribución de tamaño de partícula) del catalizador fueron realizados.

Se estudió también el efecto de solventes en el reactor semi-batch. Se investigó diferentes solventes con constantes dieléctricas ( $\epsilon$ ) entre 2 y 25. El exceso enantiomérico (ee) se incrementó a medida que se incrementó la constante dieléctrica hasta llegar a un máximo, luego presentó un decrecimiento no lineal. Se propuso un modelo cinético para la dependencia de la enantioselectividad en función de la constante dieléctrica basado en el modelo de Kirkwood. La dependencia no-lineal de ee sobre ( $\epsilon$ ) fue descrita exitosamente.

Se realizaron diferentes experimentos cinéticos sistemáticos en el reactor semi-batch. Basado en estos resultados, se desarrolló un modelo cinético asumiendo un modelo con número distintos de sitios. Las energías de adsorción de EBF sobre Pt(1 1 1) puro fueron estimadas por la teoría funcional de la densidad. Las constantes cinéticas de hidrogenación fueron determinadas junto con los parámetros de adsorción mediante una regresión numérica no-lineal. Una comparación entre el modelo y los valores experimentales reveló una muy buena aproximación.

Experimentos transitorios realizados en un reactor de lecho fijo fueron obtenidos en este trabajo. Los resultados demostraron que la continua hidrogenación enantioselectiva de EBF en hexano/2-propanol 90/10 (v/v) es posible y que la alimentación continua de (-)-cinchonidin es necesaria para mantener una alta enantioselectividad en estado estacionario. El catalizador mostró estabilidad y se logró alcanzar alta enantioselectividad en el reactor de lecho fijo.

Se estudió la separación cromatográfica de (*R*)- y (*S*)- mandelato de etilo proveniente de una mezcla del reactor continuo. Una columna comercial compuesta de una resina quiral fue escogida como adsorbente a escala preparativa. Debido a que las isotermas de adsorción fueron lineales en todo el rango de concentraciones utilizadas, estas fueron estimadas mediante pulsos experimentales para ambos isómeros provenientes de la mezcla en el reactor continuo. Las curvas de rupturas fueron medidas y descritas satisfactoriamente por un modelo disperso de flujo pistón con una aproximación lineal de fuerza impulsora.

La idea principal de este proyecto de investigación fue desarrollar un nuevo concepto integrado de producción de químicos ópticamente activos a través de catálisis heterogénea y separación cromatográfica. Este trabajo de investigación es fundamental para la tecnología avanzada de procesos, la cual busca mejorar la eficiencia y permitir la producción limpia de productos químicos enantioméricamente puros.

## LIST OF RELATED PUBLICATIONS AND PRESENTATIONS

- I. **Martin, G.**; Mäki-Arvela, P.; Murzin, D. Yu.; Salmi, T. (2014). Kinetics and catalyst deactivation in the enantioselective hydrogenation of ethyl benzoylformate over Pt/Al<sub>2</sub>O<sub>3</sub>. *Catalysis Science and Technology*. (4) 170-178.
- II. **Martin, G.**; Mäki-Arvela, P.; Murzin, D. Yu.; Salmi, T. (2013). Solvent effects in the enantioselective hydrogenation of ethyl benzoylformate. *Catalysis Letters*. (143) 1051-1060.
- III. **Martin, G.**; Mäki-Arvela, P.; Wärnå J.; Honkala, K.; Murzin, D. Yu.; Salmi, T. Kinetic modeling of ethyl benzoylformate enantioselective hydrogenation over Pt/Al<sub>2</sub>O<sub>3</sub>. *Chemical Engineering Journal* (2014) submitted
- IV. **Martin, G.**; Mäki-Arvela, P.; Murzin, D. Yu.; Salmi, T. Enantioselective hydrogenation of ethyl benzoylformate, from mechanism and kinetics to continuous reactor technology. *Topics in Catalysis* (2013) submitted.
- V. **Martin, G.**; Pereira, C.; Pettersson, F.; Saxén, H.; Murzin, D. Yu.; Rodrigues, A.; Salmi, T. Chromatographic separation of (*R*)- and (*S*)-ethyl mandelate using tris-[3,5-dimethylphenyl] carbamoyl cellulose as a chiral selector. *Chemical Engineering Research and Design* (2014) submitted.
- VI. **Martin, G.**; Kirilin, A.; Mäki-Arvela, P.; Murzin, D. Yu.; Salmi, T. Racemization of secondary alcohols over heterogeneous Ru-catalysts. (2011) Nova Science Publishers, Inc. In: *Ruthenium: Properties, Production and Applications*. 125-155 Hauppauge, NY.

## LIST OF RELATED PRESENTATIONS

- Mäki-Arvela, P.; **Martin, G.**; Simakova, I.; Tokarev, A.; Wärnå, J.; Hemming, J.; Holmbom, B.; Salmi, T.; Murzin, D. Yu. (2009) Kinetics, catalyst deactivation and modeling in the hydrogenation of sitosterol to sitostanol over micro- and mesoporous carbon supported Pd catalysts, *Chemical Engineering Journal*, (154) 45-51.
- Salmi, T.; Murzin, D. Yu.; Wärnå, J.; Mäki-Arvela, P.; **Martin, G.** (2013) Integrated modeling of reaction and catalyst deactivation kinetics—Hydrogenation of sitosterol to sitostanol over a palladium catalyst. *Chemical Engineering Science*. (104) 156–165.
- **Martin, G.**; Mäki-Arvela, P.; Murzin, D. Yu.; Salmi, T. Kinetics and catalyst deactivation in the enantioselective hydrogenation of ethyl benzoylformate over Pt/Al<sub>2</sub>O<sub>3</sub>. 12<sup>th</sup> Eurasia Conference on Chemical Science. April 16-21, 2012. Corfu, Greece. (Oral presentation)
- **Martin, G.**; Mäki-Arvela, P.; Murzin, D. Yu.; Salmi, T. Solvent effects in the enantioselective hydrogenation of ethyl benzoylformate. International symposium on catalysis and specialty chemicals ISCSC. September 23-26, 2012. Tlemcen, Algeria. (Oral presentation)
- **Martin, G.**; Mäki-Arvela, P.; Murzin, D. Yu.; Salmi, T. Solvent effects in the enantioselective hydrogenation of ethyl benzoylformate. 15<sup>th</sup> Nordic Symposium on Catalysis. June 10-12, 2012. Åland, Finland. (Poster presentation)
- **Martin, G.**; Mäki-Arvela, P.; Murzin, D. Yu.; Salmi, T. Solvent effects and modeling in the enantioselective hydrogenation of ethyl benzoylformate. 15<sup>th</sup> International Congress of Catalysis ICC. July 1-6, 2012. Munich, Germany. (Oral Presentation)
- **Martin, G.**; Mäki-Arvela, P.; Murzin, D. Yu.; Salmi, T. Batchwise and continuous hydrogenation of ethyl benzoylformate in catalytic three-phase reactors. 10<sup>th</sup> Congress on Catalysis Applied to Fine Chemicals. June 16-19, 2013. Turku/Åbo, Finland. (Poster presentation)
- **Martin, G.**; Mäki-Arvela, P.; Murzin, D. Yu.; Salmi, T. Batchwise and continuous hydrogenation of ethyl benzoylformate in catalytic three-phase reactors. 11<sup>th</sup>

European Congress on Catalysis – EuropaCat-XI, September 1-6, 2013. Lyon, France. (Poster presentation)

- **Martin, G.;** Mäki-Arvela, P.; Murzin, D. Yu.; Salmi, T. Enantioselective hydrogenation of ethyl benzoylformate, from mechanisms and kinetics to continuous reactor technology. 25<sup>th</sup> Conference of the Organic Reactions Catalysis Society ORCS. March 2-6, 2014. Tucson, Arizona. USA. (Poster presentation)
- **Martin, G.;** Mäki-Arvela, P.; Murzin, D. Yu.; Salmi, T. Continuous reactor technology in the production of optically pure compounds by enantioselective hydrogenation. 9<sup>th</sup> international symposium on Catalysis in Multiphase Reactors & 8<sup>th</sup> International Symposium on Multifunctional Reactors. December 7-10, 2014. Lyon, France.

## Table of Contents

<b>1 INTRODUCTION .....</b>	<b>1</b>
1.1 General aspects .....	1
1.2 Separation of racemates .....	2
1.3 Asymmetric hydrogenation .....	2
1.4 Research strategy .....	3
<b>2 EXPERIMENTAL SECTION.....</b>	<b>6</b>
2.1 Raw material purification .....	6
2.2 Hydrogenation in batch reactor .....	6
2.2.1 Solvent effect .....	7
2.3 Hydrogenation in fixed bed reactor .....	7
2.4 Chromatographic separation.....	8
2.5 Analytical procedures .....	9
2.5.1 Gas chromatography analysis (GC).....	9
2.5.2 Optimal emission spectrometry (ICP-OES) and Induced coupled plasma- mass spectrometer (ICP-MS). .....	10
2.6 Ultraviolet visible spectrometer .....	10
2.7 Catalyst characterization.....	11
2.7.1 Catalyst particle size measurements .....	11
2.7.2 Scanning electron microscopy (SEM).....	11
2.7.3 Nitrogen physisorption .....	11
2.7.4 Temperature programmed reduction (TPR) .....	11
2.8 Quantum chemical calculations .....	12
2.8.1 Density functional theory calculations .....	12
2.9 Racemization .....	12
2.10 Calculation of enantioselectivity and enantiomeric excess .....	12
<b>3 RESULTS AND DISCUSSION.....</b>	<b>14</b>
3.1 Catalyst characterization.....	14
3.2 ICP-OES and MS .....	16

3.3	Qualitative kinetics .....	17
3.3.1	The effect of the catalyst amount .....	17
3.4	External mass transfer .....	19
3.5	Internal mass transfer.....	20
3.6	Modifier effect.....	20
3.7	Reactant purification with activated carbon (AC).....	22
3.8	Temperature effect on the reaction rate and selectivity.....	23
3.9	Hydrogen pressure effect.....	23
3.10	Solvent effect.....	24
3.10.1	Initial rate and conversion .....	24
3.10.2	Enantioselectivity .....	25
3.10.3	Influence of ethyl acetate and 2-propanol mixtures .....	25
3.11	DFT results .....	26
3.12	Modeling results .....	29
3.12.1	Hydrogenation rates.....	29
3.12.2	Components generation rates and mass balances .....	30
3.12.3	Parameter estimation procedure .....	31
3.12.4	Results from parameter estimation.....	31
3.12.5	Solvent effect extension.....	34
3.13	Continuous hydrogenation.....	36
3.13.1	Residence time distribution .....	37
3.13.2	Dependence on the (-)-cinchonidine concentration.....	38
3.13.3	Transient experiments.....	38
3.14	Chromatographic separation.....	40
3.14.1	Adsorption of modifier by tris-[3,5-dimethylphenyl] carbamoyl cellulose .....	40
3.14.2	Pulses and breakthrough experiments .....	40
3.14.3	Mathematical model .....	42
3.14.4	Simulated moving bed operating conditions .....	44
3.15	Racemization results.....	45
<b>4</b>	<b>CONCLUSIONS .....</b>	<b>46</b>

5	<b>NOTATION</b> .....	<b>48</b>
6	<b>REFERENCES</b> .....	<b>50</b>
7	<b>PUBLICATIONS</b> .....	<b>53</b>

# 1 INTRODUCTION

## 1.1 General aspects

Chirality (handedness) is a key element in nature (Hegstrom, 1990). Because of their asymmetry, a wide range of organic substances consist of two non-superimposable mirror-image structures called enantiomers (Fig. 1). Their physical and chemical properties are identical in an achiral environment. In a chiral environment, enantiomers can react and interact in a completely different way. Life itself is full of chirality depending to a high extent on chiral recognition. A variety of biological functions are done by receptors which recognize only one enantiomer and not the second one.

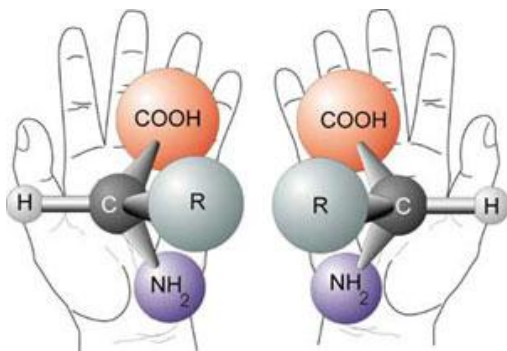


**Figure 1.** General representation of two enantiomers structures.

Nowadays, many pharmaceuticals entering the market are optically pure molecules due to their rather complex structures. Instead of selling them as racemates, which are easy and inexpensive to produce, legislation requires production of only effective optical isomers. In 1990, among the 20 most sold pharmaceuticals, 16 were optically active and 10 were delivered in an optically pure form (Sheldon, 1993). In 2000, 30 % of the total worldwide sales (€ 430 billion) of pharmaceuticals consisted of single enantiomers drugs (Chemical Engineering News, 2001). Therefore, it is evident that there is a growing interest and need for production of optically active molecules on industrial scale.

The increasing demand for a variety of enantiopure chiral compounds can only be satisfied by isolation of naturally occurring substances. More and more such compounds have to be produced synthetically. However, standard transformations of substrates lead to

racemic mixture. Therefore, the main tools in the manufacture of chiral compounds are the separation of racemates or stereoselective (asymmetric) synthesis.

## 1.2 Separation of racemates

A great effort has been made in order to develop different techniques capable of separating racemates. Among these techniques, crystallization, kinetic resolution and simulated moving bed technology can be mentioned.

Crystallization is the oldest method for separating racemates and was first described by Louis Pasteur in 1848 (Pasteur, 1848). However, separation of most chiral compounds in a racemic mixture is not possible by simple crystallization. Kinetic resolution is based on the fact that enantiomers react at different reaction rates with a chiral entity. In an ideal case, one enantiomer reacts much faster than the other one ( $k_R \gg k_S$ ). The reaction can be stopped at any time; however, it is worth stopping it at higher conversions to obtain the product with a maximum optical purity. Finally, simulated moving bed (SMB) has been recognized as an efficient continuous chromatography-based technology for the separation of enantiomers (Sunjic, 2009), particularly because it can perform successful separation for low separation factors using fairly efficient columns. SMB has been used for the separation of (*R*)- and (*S*)-ethyl lactate (Pereira, 2009), making it logical to extend its application to other esters.

## 1.3 Asymmetric hydrogenation

At present, asymmetric hydrogenation is mainly carried out by employing expensive homogeneous catalysts. However, these catalysts have their limitations in large-scale industrial production and therefore, new asymmetric catalysts need to be developed. Asymmetric synthesis using modified heterogeneous catalysts has gained lots of interest in the production of optically pure chemicals in several areas, such as pharmaceuticals, nutraceuticals, fragrances and agrochemicals (Weissermel, 1997). Modified heterogeneous catalysts are industrially interesting; because some available examples have demonstrated that high enantioselectivities (>95%) close or even exceeding those obtained with existing homogeneous catalysts for the same reaction can be achieved (Izumi, 1983; Blaser, 1991).

In these catalytic systems, the source of chirality is an organic compound, commonly named chiral modifier, which adsorbs strongly on the catalyst surface and creates a chiral environment for the enantioselective hydrogenation. The reactants can interact with the metal and the chiral modifier simultaneously and be transformed to the desired product.

The hydrogenation of  $\alpha$ -ketoesters on supported Pt catalysts modified with cinchona alkaloids was discovered by Orito *et al* in 1979 (Orito, 1979) and, since then, detailed studies have been conducted and different substrates have been investigated using Pt-cinchona alkaloid catalytic systems. High enantiomeric excesses have been obtained in many cases, i.e. for ketopantolactone ( $ee > 90\%$ ) (Schürch M. S., 1997), (Schürch M. K., 1998),  $\alpha$ -keto acetals ( $ee > 95\%$ ) (Studer, 1999), ethyl-4,4-dimethylpyrrolidine-2,3,5-trione ( $ee > 90\%$ ) (Künzle, 1998), trifluoro- $\beta$ -ketoester ( $ee = 90\%$ ) (von Arx, 2000), 2,2,2-trifluoroacetophenone ( $ee = 56\%$ ) (Mallat, 1997), (Bodmer, 1998) and  $\alpha$ -ketoamides ( $ee_{max} = 60\%$ ) (Wang, 1997).

Solvents have a crucial effect in the production of fine chemicals. Although the presence of solvents in the reaction mixture increases the process costs, the use of solvents in liquid-phase reactions is required to accomplish at least one of the following functions: 1) to dissolve solid reactants and products; 2) to control the reactant rate in the case of very rapid chemical reactions; 3) to dissipate the heat generated in highly exothermic reactions. The choice of suitable solvents is frequently critical and an unfortunate choice can lead to a loss of activity and/or selectivity. Therefore, the selection of solvents is extremely important to understand how solvents interact with the reaction components.

#### 1.4 Research strategy

The main target of this project is the research and development of a new integrated concept for the production of optically active chemicals by using heterogeneous asymmetric catalyst and chromatographic separation (Fig. 3). The catalyst, reaction and separation conditions are integrated and optimized in order to enable a sustainable and feasible continuous process. Hydrogenation of ethyl benzoylformate (EBF, A) to (*R*)- and (*S*)- ethyl mandelate (B, C) in a presence of (-)-cinchonidine (M) as a catalyst modifier was studied as a model system. The reaction scheme is displayed in Fig. 2.

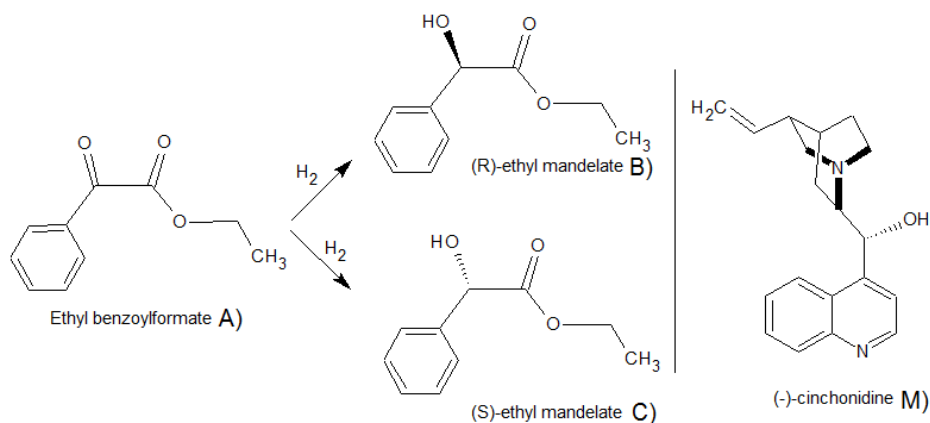


**Figure 2.** Reaction scheme for the hydrogenation of EBF and the catalyst modifier (M), (-)-cinchonidine (Toukoniitty E, 2010).

The kinetic studies were carried out in a semi-batch and fixed-bed reactors. The reaction kinetic was explored experimentally and optimized quantitatively [I, II, IV]. The separation experimental part started with a construction of a chromatographic separation unit operating in a batch mode [V]. In this column, several flow rates and inlet concentration of enantiomers were tested.

In addition to all the experimental activities, modeling studies were carried out in parallel to the laboratory work [II, III, V]. Publication II described the influence of solvent dielectric coefficients in the enantiomeric excess and initial hydrogenation rate. The kinetics of enantioselective hydrogenation considering the influence of amount of modifier, temperature and hydrogen pressure was analyzed in publication III. Publication V accounts for the separation in a simulating moving bed influenced by flow rate initial concentration. The models provided good predictions of the experimental values in all cases.

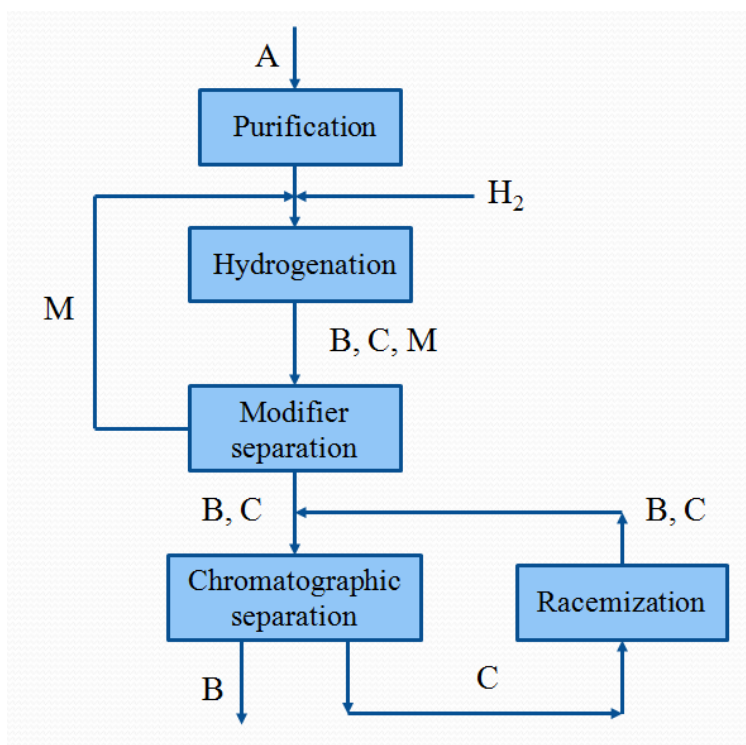


**Figure 3.** Research strategy

## 2 EXPERIMENTAL SECTION

### 2.1 Raw material purification

Since the raw material (EBF, Aldrich, 95%, 25, 891-1) contained sulfurous impurities (up to 2%, [I]), EBF was treated in some experiments with 220 mg of activated carbon (Chemviron Carbon, IVP, FE 51012A) for 2 h prior to its use [I].

### 2.2 Hydrogenation in batch reactor

Hydrogenation experiments were performed in a glass reactor at atmospheric pressure under a flow of molecular  $H_2$  with a volumetric flow rate of 295 ml/min at 25 °C (Fig. 4). The selected temperatures were 0, 25 and 50 °C. The hydrogenation catalyst (5% (w/w) Pt/ $Al_2O_3$  Aldrich, Strem, 78-1660) was pre-reduced under flowing hydrogen at 400°C for 2 h. To avoid interactions between catalyst and oxygen, the reaction medium was bubbled with Ar for 10 min before putting it in contact with the catalyst. To study external mass transfer limitations, different stirring rates were tested (250, 500 and 750 rpm). The internal mass-transfer resistance was overcome by using small catalyst particles ( $< 90 \mu m$ ). The liquid-phase volume and the initial concentration of the substrate (A) were 150 mL and 5.6 mmol/L, respectively. (-)-Cinchonidine (M) was used as a catalyst modifier with a concentration between 0 and 0.005 mol/L. The hydrogen partial pressure was varied between 0.4 and 1 bar. The mass of the catalyst was 220 mg [I].

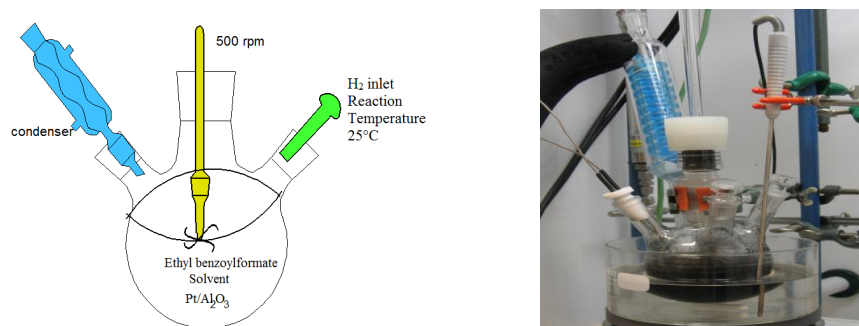


**Figure 4.** Batch reactor set-up: process diagram (left) and photo (right)

### 2.2.1 Solvent effect

Several solvents with dielectric constants ( $\epsilon$ ) in the range of 2-25 were investigated. In order to obtain a more detailed insight into the influence of  $\epsilon$ , two solvents (2-propanol and ethyl acetate) were mixed in different proportions (25-75, 50-50 and 75-25 %) and subsequently tested. The dielectric constants and hydrogen solubility in different solvents have been previously measured (Toukoniitty E, 2003). Toluene (J.T. Baker, 8077, >99.5%), ethyl acetate (LAB-SCAN, 99.8%), methyl acetate (Acros, 99%), tetrahydrofuran (LAB-SCAN, 99.8%), 1-pentanol (Fluka, 98%), 1-propanol (Sigma-Aldrich, 99.5%, 402893) 2-propanol (LAB-SCAN, 99.7%), ethanol (Primalco, 99.5%), methyl cyclohexane (Fluka, >98%, 66295), 1-octanol (Riedel-de Haën, 99.5%, 24134), acetone (J.T. Baker, 99.5%) and (-)-cinchonidine (Fluka, 27350, 98%) were used as received [III].

### 2.3 Hydrogenation in fixed bed reactor

The experiments were performed in a continuous up-flow fixed bed reactor (47 cm length and 3 cm internal diameter) at atmospheric pressure under a flow of molecular  $H_2$  with a volumetric flow rate of 295 ml/min at 25 °C (Fig. 5). The selected temperatures were -20, -10, 0 and 25 °C. Hexane/2-propanol (90/10) v/v was used as the reaction solvent. The hydrogenation catalyst was 1% (w/w) Pt/ $Al_2O_3$  (3.2 mm pellets, Aldrich). The catalyst was placed inside the reactor with quartz balls (67 g, diameter 3 mm and density 2687 [ $kg\ m^{-3}$ ]). To avoid interactions between the catalyst and oxygen, the reaction medium was bubbled with Ar for 10 min before putting it in contact with the catalyst. (-)-Cinchonidine was used as a catalyst modifier with a concentration between 0 and 0.041 mmol/L. The liquid phase volume and the initial concentration of EBF were 0.9 L and 5.6 mmol/L, respectively. Typically, the experiments were carried out with co-current gas and liquid flows ( $5\ cm^3\ min^{-1}$ ) [IV].

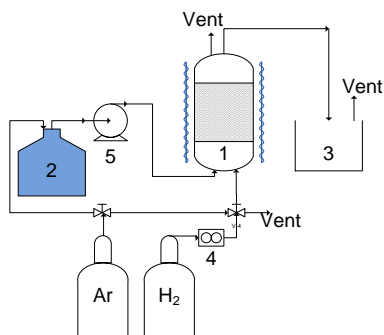


**Figure 5.** Scheme of the continuous reactor set-up. 1) Continuous flow reactor, 2) substrate vessel, 3) product vessel, 4) mass flow controller and 5) substrate pump.

The residence time distribution in the fixed bed reactor was investigated by applying step changes using ethyl benzoylformate in hexane/2-propanol (90/10) v/v. In order to measure the axial dispersion effects in a reliable manner by blocking the catalyst pores, the catalyst was sprayed three times with a resin (Dupli Color RAL7035) and dried for 24 h each time. The experiments were performed at room temperature (25 °C). Before the experiment was started, the column was fed with solvent for 10 min. A step experiment with a concentration 0.0056 mol/L of EBF was fed to the column for 100 min. The samples were collected every 2 minutes time-on-stream the first 40 minutes and then every 5 minutes up to the steady-state [IV].

## 2.4 Chromatographic separation

A preparative column filled with tris-[3,5-dimethylphenyl] carbamoyl cellulose coated on a 10 µm silica gel substrate was used as chromatographic medium supplied by Scantec Lab Stockholm, Sweden. The length of the column (L) and the volume of the bed (V) were 25 cm and 19.63 cm<sup>3</sup>, respectively. The pore size was larger than 100 nm. The structural unit of the packing composition is shown in Fig. 6.

Online concentration analysis was conducted using a high-performance liquid chromatograph (HP 1100 Series LC) coupled to a UV detector (HP 1100 Series G1314A) at 270 nm. The employed method consisted of a 100 µL sample injection and mobile phase flows of 0.5, 1 and 1.5 mL min<sup>-1</sup> at 25 °C [V].

Elution chromatography experiments with non-retained species were performed to determine the bulk porosity of the preparative chiral column. The chromatographic peaks for the unretained tracer (1,3,5-Tri-tert-butylbenzene (TTBB)) were obtained at flow rates from 0.5, 1.0 and 1.5 cm<sup>3</sup>/min using a mixture of hexane/2- propanol (90/10) as a mobile phase. In the case of single-component breakthrough curves, the flow rate equal to 1.0 cm<sup>3</sup>/min and concentrations of enantiomers 0.5, 4.65 and 9.3 g/L were used.

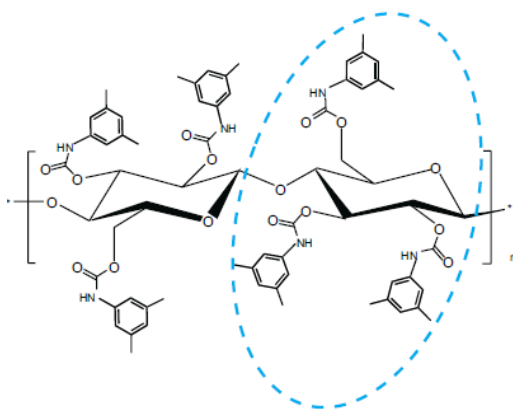


**Figure 6.** The structural unit of the chiral adsorbent tris-(3,5-dimethylphenyl) carbamoyl cellulose (AB, 2007).

## 2.5 Analytical procedures

### 2.5.1 Gas chromatography analysis (GC)

Samples were withdrawn from the batch reactor at different time intervals and analyzed with a gas chromatograph (GC) (Varian 3300) equipped with a chiral column (Silica Chirasil-DEX; length 25 m, diameter 0.25 mm, film thickness 0.25  $\mu$ m). Helium was used as a carrier gas with a split ratio of 33. The flame ionization detector (FID) and injector temperatures were 270 and 240°C, respectively. The temperature program of the GC was 120°C (25 min)–20°C/min–190°C (6 min). The GC analysis was calibrated with ethyl benzoylformate (Aldrich, 95%, 25,891-1), (*R*)-ethyl mandelate (Aldrich, 99%, 30,998-2) and (*S*)-ethyl mandelate (Aldrich, 99%, 30,997-4). In the case of the continuous

reactor, samples were collected at the outlet at different time intervals during 200 min of reaction [I, II, IV].

### **2.5.2 Optimal emission spectrometry (ICP-OES) and Induced coupled plasma- mass spectrometer (ICP-MS).**

The content of Pt in the Pt/Al<sub>2</sub>O<sub>3</sub> (3.2 mm pellets, Aldrich) was measured by a PerkinElmer, Optima 5300 DV Inductively plasma optimal emission spectrometry (ICP-OES). The sample was digested with two different acid combinations. The first sample was digested in 5 ml aqua regia ( 3:1 HCl:HNO<sub>3</sub> ) and the second was digested in 3 ml H<sub>2</sub>SO<sub>4</sub>(96%) + 3 ml HNO<sub>3</sub>(65%). A multi-element standard was used as a calibration solution and the Pt was measured at 265.945 nm.

Additionally, the presence of metals in the raw material was measured by a Perkin Elmer-Sciex Elan 610 DRC Plus Inductively Coupled Plasma Mass Spectrometry (ICP-MS). The instrument operates at the nebulizer flow of 0.8 ml/min and the auxiliary gas flow of 0.2 ml/min, respectively. Plasma gas flow was 1.5 ml/min with the plasma power of 1300 W. The samples were digested before the measurements; in this case approximately 100 mg of ethyl benzoylformate was weighed into a teflon bomb and 5 ml HNO<sub>3</sub> (65 %) and 1 ml H<sub>2</sub>O<sub>2</sub> (30 %) were added. The solution was digested in a microwave oven (Anton Paar, Multiwave 3000) and diluted to 100 ml with deionized water. A multi-element standard was used as a calibration solution and the samples were diluted by a factor of 5 prior to the measurements. Sulfur was measured at 181.975 nm and phosphorus was analyzed in a semiquantitative mode (rsd ≤ 25 %) [I].

### **2.6 Ultraviolet visible spectrometer**

UV-spectra were registered to measure the (-)-cinchonidine adsorption on the tris-[3,5-dimethylphenyl] carbamoyl cellulose. For this purpose, a UV-spectrometer with the following conditions was used: Shimadzu UV-2550 UV-VIS spectrometer with an UV lamp (305-318 nm).

## **2.7 Catalyst characterization**

### **2.7.1 Catalyst particle size measurements**

The mean particle size of the commercial catalyst (5% (w/w) Pt/Al<sub>2</sub>O<sub>3</sub> Aldrich, Strem, 78-1660) was measured with a Malvern Zetasizer IIC apparatus. The catalyst was suspended in water and the solution was stirred with a magnet. The size measurement was based on the scattering of He-Ne light, which was reflected to a catalyst powder-water suspension. The interference figures of the scattered light were collected by a Fourier lens and reflected to the detector. The interference images were processed by the computer unit of the measurement apparatus to calculate the corresponding catalyst particle size distribution on the basis of the light intensity variation of the figures [I].

### **2.7.2 Scanning electron microscopy (SEM)**

Catalyst images as well as elemental analyses were obtained with a Leo Gemini 1530 scanning electron microscope equipped with a ThermoNORAN Vantage X-ray detector for EDXA analysis. The images were taken using the Secondary Electron and Backscattered Electron detectors at 15 kV, and the In-Lens Secondary Electron detector at 2.70 kV [I].

### **2.7.3 Nitrogen physisorption**

The specific surface area was measured by Sorptomatic 1900, Carlos Erba Instruments. The catalyst was degassed for 4 h at 300 °C in vacuo prior to the surface area measurement by nitrogen adsorption. The data were interpreted with the Brunauer-Emmett-Teller (BET) isotherm [I].

### **2.7.4 Temperature programmed reduction (TPR)**

The metal dispersion was determined by CO pulse-chemisorption method in an Autochem 2900 apparatus manufactured by Micromeritics Ltd. The catalyst was reduced prior to the measurement with the following programme: 25–50 °C, at 10 °C/min in helium, dwell for 30 min, gas-switch to hydrogen, 5 °C/min to 250 °C and dwell for 2 h followed by flushing for 60 min in helium at 250 °C. Thereafter, the catalyst was cooled down to ambient temperature and pulses of CO were introduced utilizing 10 vol.% CO in helium.

The stoichiometry 1:1 for Pt:CO was assumed (Tokarev, 2010). The temperature programmed reduction (TPR) of the catalyst was performed with the above mentioned Autochem instrument using the following temperature programme: 5 C/min – 400°C for Pt/Al<sub>2</sub>O<sub>3</sub>. The carrier gas was a mixture of 5% of hydrogen in argon with flow rate of 30 ml/s [I].

## 2.8 Quantum chemical calculations

### 2.8.1 Density functional theory calculations

Density functional theory (DFT) calculations were carried out for ethyl benzoylformate (EBF) adsorption on a Pt(111) surface employing the GPAW (Enkovaara, 2010) implementation of the projected augmented wave method (Blöchl, 1994) in real space grid. The grid spacing was 0.2 Å for all directions. The exchange and correlation functional was approximated with BEEF-vdW (Wellendorff, 2012) formula that includes description for dispersion effects. The platinum surface was modelled with a 4-layer thick slab which is periodic in x- and y-directions and has a (4x3) surface unit cell. All the other atomic positions were relaxed till residual force was below 0.05 eV/Å but the bottom metal layer was fixed to its ideal bulk positions. The Brillouin zone was sampled using a 2x4 grid of k-points [III].

## 2.9 Racemization

The racemization of (*S*)-ethyl mandelate towards (*R*)-ethyl mandelate was performed in a glass reactor at atmospheric pressure under a flow of molecular Ar with a volumetric flow rate of 295 ml/min at 80 °C. The racemization catalyst was (5 wt% Ru/Al<sub>2</sub>O<sub>3</sub> Aldrich, Degussa type H213 R/D). To avoid interactions between catalyst and oxygen, the reaction medium was bubbled with Ar for 10 min before putting it in contact with the catalyst. The stirring rate was 500 rpm and the catalyst was unsieved. The liquid-phase volume and the initial concentration of the substrate (C) were 150 mL and 5.6 mmol/L, respectively. The mass of the catalyst was 220 mg [II].

### 2.10 Calculation of enantioselectivity and enantiomeric excess

The enantiomeric excess (ee) was calculated using the following equation:

$$ee = \frac{|C_B - C_C|}{(C_B + C_C)} \times 100\% \quad (1)$$

where  $C_B$  and  $C_C$  denote the concentration of (*R*)-ethyl mandelate and (*S*)-ethyl mandelate respectively. The enantioselectivity (*es*) was calculated as follows:

$$es = \frac{C_B}{C_C} \times 100\% \quad (2)$$

### 3 RESULTS AND DISCUSSION

#### 3.1 Catalyst characterization

The metal dispersion of the catalyst was investigated by CO pulse chemisorption. For Pt/Al<sub>2</sub>O<sub>3</sub> (5% (w/w) Aldrich, Strem, 78-1660), the metal dispersion was 34%, which corresponds to an average platinum metal nanoparticle size of 3 nm. The metal crystal size close to 3 nm was found to be appropriate for a high chiral induction in the hydrogenation of  $\alpha$ -ketoesters [I].

The temperature-programmed reduction profile of the catalyst showed three peaks, at 75, 180, and 350 °C (Fig. 7). The first two peaks can be attributed to the reduction of the Pt particles to their metallic state, whereas the peak observed at 350 °C is not caused by reduction of Pt and its intensity depends on the amount of carrier and not on the amount of Pt. Some phase changes might also take place both in the support material and in the Pt-phase (Lieske, 1983).

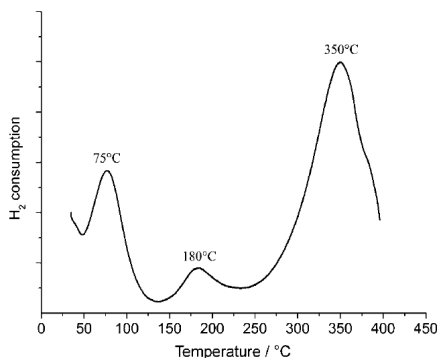


**Figure 7.** Temperature-programmed reduction profile of 5 wt% Pt/Al<sub>2</sub>O<sub>3</sub>

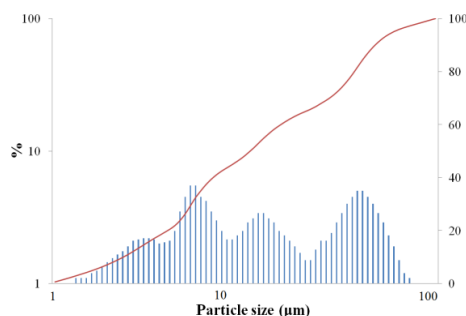


**Figure 8.** Pt particle size distribution in 5 wt% Pt/Al<sub>2</sub>O<sub>3</sub>

The mean Pt/Al<sub>2</sub>O<sub>3</sub> catalyst particle size was 15.9  $\mu\text{m}$  (Fig. 8) and the morphology of the catalyst particle is visible from Fig. 9. Additionally, the largest particles were about 40.8  $\mu\text{m}$ , whereas the smallest particles were ca. 2.8  $\mu\text{m}$ . The specific surface area and the pore volume of the fresh catalyst determined by nitrogen adsorption were 95  $\text{m}^2/\text{g}_{\text{cat}}$  and 0.319  $\text{cm}^3/\text{g}_{\text{cat}}$ , respectively.

**Table 1.** Elemental composition of fresh and spent Pt/Al<sub>2</sub>O<sub>3</sub> measured by EDX.

Fresh Pt/Al <sub>2</sub> O <sub>3</sub>							
	<b>O</b>	<b>Al</b>	<b>F</b>	<b>Si</b>	<b>K</b>	<b>Pt</b>	<b>S</b>
<b>Weight (%)</b>	51	43	-	-	-	6	-
<b>Weight % Error (+/-)</b>	0.4	0.2	-	-	-	0.2	-
<b>Atom %</b>	66	33	-	-	-	1	-
<b>Atom % Error (+/-)</b>	0.6	0.1	-	-	-	0.02	-
<b>Compound (%)</b>	51	43	-	-	-	6	-

Spent Pt/Al<sub>2</sub>O<sub>3</sub>. The raw material was **not** purified with activated carbon before the reaction

<b>Weight (%)</b>	47	46	0.6	-	-	5.6	0.77
<b>Weight % Error (+/-)</b>	0.4	0.1	0.2	-	-	0.3	0.09
<b>Atom %</b>	62	36	0.7	-	-	0.78	0.52
<b>Atom % Error (+/-)</b>	0.5	0.1	0.2	-	-	0.03	0.06
<b>Compound (%)</b>	47	46	0.6	-	-	5.6	0.77

Spent Pt/Al<sub>2</sub>O<sub>3</sub>. The raw material was purified with activated carbon before the reaction

<b>Weight (%)</b>	49	44	0.29	0.16	0.15	6.4	-
<b>Weight % Error (+/-)</b>	0.4	0.2	0.04	0.04	0.04	0.2	-
<b>Atom %</b>	64	35	0.2	0.10	0.06	0.64	-
<b>Atom % Error (+/-)</b>	0.5	0.1	0.04	0.03	0.02	0.02	-
<b>Compound (%)</b>	49	44	0.29	0.16	0.15	6.4	-

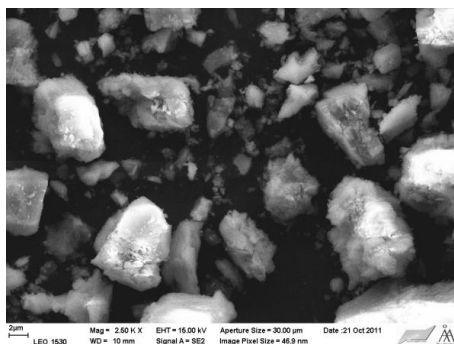


**Figure 9.** SEM image of the fresh Pt/Al<sub>2</sub>O<sub>3</sub>.

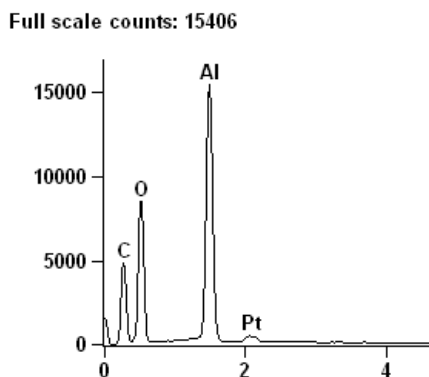


**Figure 10.** EDX analysis for the fresh Pt/Al<sub>2</sub>O<sub>3</sub>.

The results from the EDX-analysis (Fig. 10) showed that the main components present in this catalyst were Pt (6.2 %), Al (42.6 %) and O (51.2 %) (Table 1). The EDX analysis results showed that there was neither sulfur nor any other poisoning agent present in the fresh Pt/Al<sub>2</sub>O<sub>3</sub> catalyst. However, the results in the spent catalyst revealed (Table 1) that sulfur and fluorine were introduced, when unpurified raw material was used.

### 3.2 ICP-OES and MS

The concentration of sulfur was around 2% w/w for unpurified ethyl benzoylformate. Table 2 contains the calculated amounts of Pt loaded in the reactor at different catalyst masses and the respective sulfur-to-platinum ratios.

**Table 2.** Amount of Pt in Pt/Al<sub>2</sub>O<sub>3</sub>

<i>Amount of cat (mg)</i>	<i>Amount of surface Pt (mol)</i>	<i>Ratio S/surface Pt *</i>
110	$9.59 \times 10^{-6}$	9.8
220	$1.92 \times 10^{-5}$	4.9
440	$3.84 \times 10^{-5}$	2.4

\* This amount refers to 134.8 µL of EBF

These calculations refer only to the surface Pt and not accounting for the catalyst support. It was not possible to estimate the distribution of sulfur on the catalyst, leading to

the uncertainty about how much sulfur was in reality adsorbed on Pt or on the support. Nevertheless, these characterization results explain the poor conversion and ee when the amount of catalyst was less than 165 mg (Section 3.3.1). These results confirmed that it was absolutely necessary to purify the raw material before its use.

The results from ICP-OES for the content of Pt in the Pt/Al<sub>2</sub>O<sub>3</sub> (3.2 mm pellets, Aldrich) are shown in Table 3. Both digestion processes showed approximately an 1 % Pt content which is in accordance with the data supplied by the catalyst manufacturer.

**Table 3.** Amount of Pt in Pt/Al<sub>2</sub>O<sub>3</sub> (3.2 mm pellets, Aldrich)

<i>Sample</i>	<i>m (g)</i>	<i>Pt (%)</i>
Pt/Al <sub>2</sub> O <sub>3</sub>	0.0473	1.0
Pt/Al <sub>2</sub> O <sub>3</sub>	0.0507	0.8

### 3.3 Qualitative kinetics

The reaction scheme for the hydrogenation of EBF (**A**) is displayed in Fig. 2. As the figure shows, the complete reaction scheme comprised three components. The reactant, ethyl benzoylformate (**A**), is hydrogenated over Pt catalyst to produce two enantiomers (*R*)- and (*S*)- ethyl mandelate, (**B**) and (**C**), respectively. All reaction components **A**, **B**, and **C** in the scheme were distinguishable by chromatographic analysis. In the presence of the chiral modifier, (-)-cinchonidine (**M**), (*R*)-ethyl mandelate is formed in excess.

#### 3.3.1 The effect of the catalyst amount

The amount of catalyst in the hydrogenation of ethyl benzoylformate was varied [**I**]. The concentration of (-)-cinchonidine was kept constant in all experiments (0.02 mmol/L).

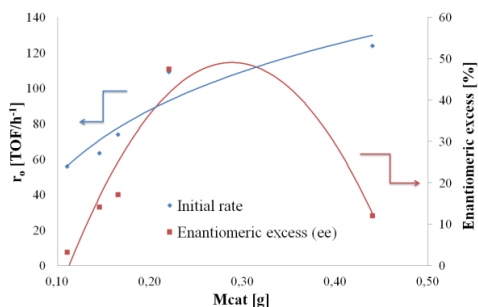


**Figure 11.** Influence of the catalyst mass on the enantioselective hydrogenation of ethyl benzoylformate. Reaction conditions: 0.85 mmol of ethyl benzoylformate, 110-440 mg of 5 wt% Pt/Al<sub>2</sub>O<sub>3</sub> (<90 μm), 150 mL of toluene, 25 °C and p<sub>H<sub>2</sub></sub> = 1 atm.

The initial rate expressed as the turnover frequency (TOF) increased as the amount of catalyst was increased which is illustrated in Fig. 11. The results showed that deactivation by sulfur occurred on the catalyst and the removal of impurities by pretreatment of the raw material was needed (Table 4, entry 3 and 4) [I]. The enantiomeric excess went up as the amount of catalyst increased up to a maximum. Then, it decreased due to an excess of the catalyst coverage which gives more places available for the racemic production.

**Table 4.** The influence of the catalyst amount on the hydrogenation of ethyl benzoylformate over Pt/Al<sub>2</sub>O<sub>3</sub>. Reaction conditions: 0.85 mmol of ethyl benzoylformate, 0.0031 mmol of CD, 110-440 (unpurified) mg of 5 wt% Pt/Al<sub>2</sub>O<sub>3</sub> (<90 μm), 150 mL of toluene, 25 °C, p<sub>H<sub>2</sub></sub> = 1 atm. and 500 rpm

<i>Mass of Cat</i> (g)	<i>Initial rate</i>	<i>Conversion (%)</i>	<i>ee (%)</i>
	(TOF/h <sup>-1</sup> )	After 24 h	
0.110	56	12	3
0.145	62	20	14
0.165	74	35	17
0.220	109	100	48
0.440	124	100	12

### 3.4 External mass transfer

The stirring rates were varied in the batch reactor in order to study external mass transfer limitations (Fig. 12). A complete reactant conversion was achieved in all the experiments after 24 hours [I].

The initial hydrogenation rate increased by 38% as the stirring rate was increased from 250 to 500 rpm but there was only 10% difference was observed when the stirring rate was increased from 500 to 750 rpm. An increase in ee of 20% was observed when the stirring rate changed from 250 to 500 rpm, but less than 5 % difference was found for stirring at 500 and 750 rpm. These results correspond to the previous studies which have proved that the enantioselective hydrogenation of  $\alpha$ -ketoesters is not influenced by external mass transfer limitations and remains on the same level as under kinetic control (Toukoniiitty E, 2003). Thus, the stirring speed of 500 rpm was considered to be sufficient for kinetic control.

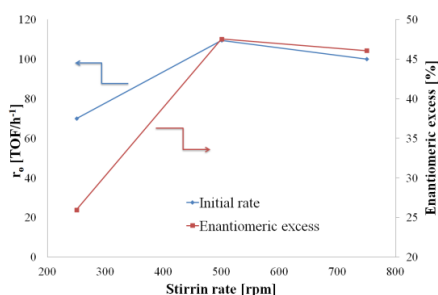


**Figure 12.** Influence of the stirring rate on the enantioselective hydrogenation of ethyl benzoylformate. The reaction conditions: 0.85 mmol of ethyl benzoylformate, 0.16 n (CD) / n (surface Pt), 220 mg of 5 wt% Pt/ $\text{Al}_2\text{O}_3$  ( $<90 \mu\text{m}$ ), 150 mL of toluene, 25 °C and  $p\text{H}_2 = 1 \text{ atm}$ .

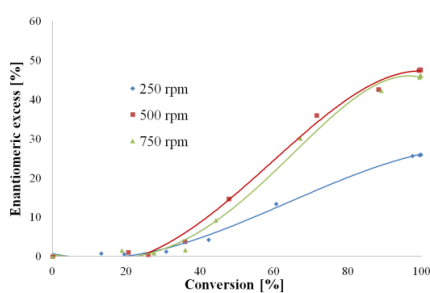


**Figure 13.** Dependence of the enantiomeric excess on the reactant conversion for different stirring rates.

Additionally, by plotting the enantiomeric excess vs. conversion (Fig. 13) an increase of enantiodifferentiation after 30 % of conversion is visible. Interactions between the product and the modifier were suggested as the explanation for this [I].

### 3.5 Internal mass transfer

The presence of internal mass transfer limitations was studied using different catalyst particle sizes (<90  $\mu\text{m}$  and unsieved) (Fig. 14). A complete reactant conversion was achieved in both experiments after 24 hours. The enantiomeric excesses for the catalyst particle size below 90  $\mu\text{m}$  and the unsieved catalyst were 48 and 56 %, respectively. This difference in ee could be explained by more sulfur tolerance of larger particles due to the stronger sulfur binding to the smaller ones (Baldyga, 2012).

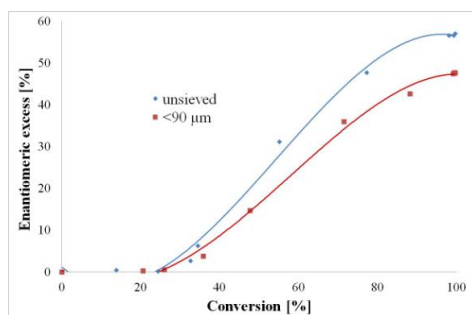


**Figure 14.** Influence of the catalyst particle size on the enantioselective hydrogenation of ethyl benzoylformate. Reaction conditions: 0.85 mmol of ethyl benzoylformate, 0.16 n (CD) / n (Surface Pt), 220 mg of 5 wt% Pt/Al<sub>2</sub>O<sub>3</sub>, 150 mL of toluene, 25 °C and hydrogen atmosphere.

### 3.6 Modifier effect

The influence of the modifier concentration on the enantiomeric excess and the initial hydrogenation rate in the batch reactor was studied using EBF as received. Toluene was used as solvent. In the absence of the modifier, the reaction led to a racemic mixture of (*R*)- and (*S*)-ethyl mandelate.

The highest enantiomeric excess (at 24 hours of the reaction) was 85% using the molar ratio of modifier-to-surface Pt of 1.28, but it varied as a function of the modifier concentration (Table 5). No variation in the ee was observed at high modifier concentrations (Table 5, entries 10 and 11) due to the solubility of the modifier in toluene [I]. It is observed that ee passed through a maximum and decreased with an increasing modifier concentration (Fig. 15).

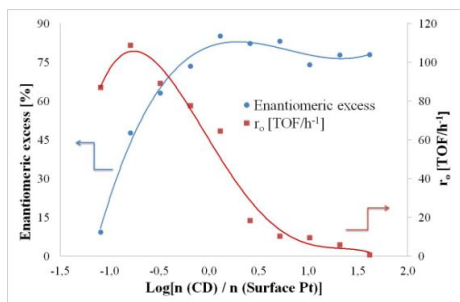


**Figure 15.** Influence of the mass of modifier on the enantioselective hydrogenation of ethyl benzoylformate. Reaction conditions: 0.85 mmol of ethyl benzoylformate, 220 mg of 5 wt% Pt/Al<sub>2</sub>O<sub>3</sub> (<90 μm), 150 mL of toluene, 25 °C, pH<sub>2</sub> = 1 atm and 500 rpm.

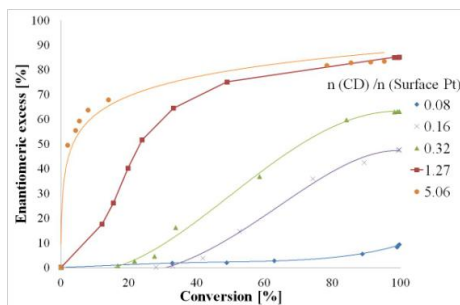


**Figure 16.** Influence of cinchonidine amount (mmol) and conversion on ee. Reaction conditions: 0.85 mmol of ethyl benzoylformate, 220 mg of 5 wt% Pt/Al<sub>2</sub>O<sub>3</sub> (<90 μm), 150 mL of toluene, 25 °C, pH<sub>2</sub> = 1 atm and 500 rpm.

**Table 5.** Influence of the mass of modifier (CD) on the hydrogenation of ethyl benzoylformate over Pt/Al<sub>2</sub>O<sub>3</sub>. Reaction conditions: 0.85 mmol of ethyl benzoylformate, 220 mg of 5 wt% Pt/Al<sub>2</sub>O<sub>3</sub> (<90 μm), 150 mL of toluene, 25 °C, pH<sub>2</sub> = 1 atm and 500 rpm.

$n (CD)/$ $n (Surface Pt)$	Initial rate (TOF/h <sup>-1</sup> )	Conversion after 24 h (%)	ee (%)
0	69	100	1
0.08	87	100	8
0.16	109	100	48
0.32	89	100	63
0.64	77	100	74
1.27	64	100	85
2.53	18	96	82
5.06	10	95	83
10.12	9	90	74
20.24	6	86	78
40.48	<1	68	78

The formation rate of the (*R*)-enantiomer rapidly increased when small amounts of modifier were introduced into the system (Table 5, entries 1 and 2). However, after a maximum the rate decreased as the modifier concentration increased up to a lower level than in the absence of the modifier (Fig. 15). From these observations it can be concluded that up to a certain optimum value of the modifier concentration, the enantioselectivity and the initial reaction rate increase; however, a further increase of the modifier concentration results in a decreasing enantioselectivity and reaction rate.

The dependence of the ee on conversion was also studied (Fig. 16). Low amounts of CD do not afford any enantiodifferentiation. However, larger amounts of the modifier led to a rapid increase of the ee and mediocre changes after it.

### 3.7 Reactant purification with activated carbon (AC)

The purification of the reactant by contacting it with a solution containing activated carbon was investigated, because severe catalyst deactivation was observed when the reactant was used as received. The amount of modifier, (-)-cinchonidine was kept constant in all experiments (0.02 mmol/L). Other purification techniques such as vacuum distillation were considered. However, the simplicity and the good results given by activated carbon in the treatment of EBF (Fig. 17) were considered to be sufficient [I].

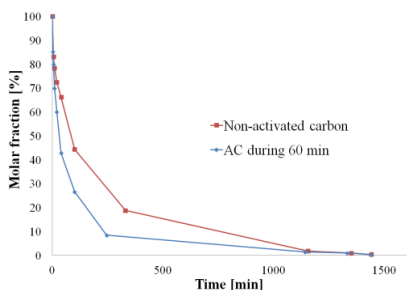


**Figure 17.** The influence of activated carbon in the conversion of ethyl benzoylformate. Reaction conditions: 0.85 mmol of ethyl benzoylformate, 0.32 n (CD) / n (Surface Pt), 220 mg of 5 wt% Pt/Al<sub>2</sub>O<sub>3</sub> (<90 μm), 150 mL of toluene, 25 °C and p<sub>H<sub>2</sub></sub> = 1

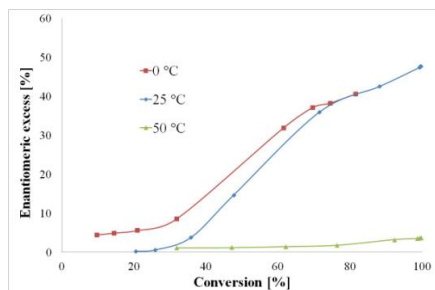


**Figure 18.** The influence of reaction temperature in the enantioselective hydrogenation of ethyl benzoylformate. Reaction conditions: 0.85 mmol of ethyl benzoylformate, 0.16 n (CD) / n (Surface Pt), 220 mg of 5 wt% Pt/Al<sub>2</sub>O<sub>3</sub> (<90 μm), 150 mL of toluene and p<sub>H<sub>2</sub></sub> = 1 atm.

The increase of the initial hydrogenation rate when activated carbon was used can be explained by adsorption of sulfur present in the substrate (Fig. 17). However, the difference concerning ee is more profound showing a decrease of 24% when activated carbon was used, which could be explained by an increase of the modifier to-substrate molar ratio ( $\theta_M/\theta_S$ ) [I].

### 3.8 Temperature effect on the reaction rate and selectivity

The influence of the reaction temperature was studied. Toluene was used as solvent. The temperature was varied between 0-50°C. The reaction temperature influenced both the initial hydrogenation rate and ee. A complete conversion was obtained for 25 and 50 °C while at 0 °C it was not reached after 24 hours. The enantiomeric excess did not change when the temperature increased from 0 to 25 °C at 80% of conversion (Fig. 18). An intense decrease in the ee was observed when the temperature was shifted from 25 to 50 °C from 48 to 3 % [I]. The effect can be explained by the adsorption equilibrium of the modifier.

A high reaction temperature is not feasible for cinchona-alkaloid modified systems, as the enantioselectivity is known to dramatically decrease at higher temperatures (<50°C) (Sutherland, 1990), which is attributed to the desorption of the modifier and temperature-induced changes in the adsorption mode of the modifier (Bürgi, 1998).

### 3.9 Hydrogen pressure effect

The effect of hydrogen pressure on the reaction rate and enantiomeric distribution was studied at different hydrogen pressures [III]. A complete reactant conversion after 24 hours was achieved for all the experiments. The initial hydrogenation rate was found to increase as the hydrogen pressure increases (Fig. 19). It was observed that the ee varied less than 10% in the whole range of pressures (Fig. 19). These results can be explained by a non-competitive Langmuir-Hinshelwood mechanism (Ruiz, 2008).

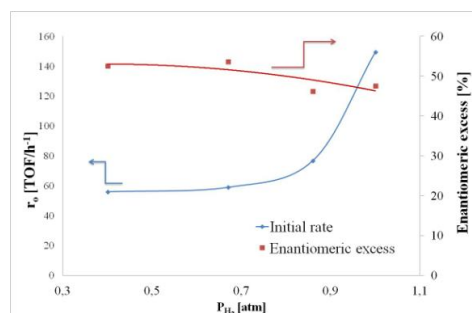


**Figure 19.** Influence of hydrogen pressure on the enantiomeric excess and initial rate. Reaction conditions: 0,85 mmol of EBF, 0.16 n (CD) / n (Surface Pt), 220 mg of 5 wt% Pt/Al<sub>2</sub>O<sub>3</sub> (<90  $\mu$ m), 150 mL of toluene and 25 °C.

### 3.10 Solvent effect

The solvent effect on the enantioselective hydrogenation of ethyl benzoylformate were studied. Three groups of solvents were studied: protic, aprotic polar and apolar. The effects of pure solvents and binary solvent mixtures on the hydrogenation rates and enantioselectivity were investigated.

#### 3.10.1 Initial rate and conversion

The initial hydrogenation rate varied in different solvents, the highest values were observed in toluene and methyl cyclohexane and the lowest ones in ethyl acetate and tetrahydrofuran, while relatively high rates were obtained in the other studied solvents. The activity pattern with the protic solvents were: 2-propanol>1-propanol>1-octanol>ethanol. In case of aprotic polar solvents, the activity followed the pattern: methyl acetate>acetone>ethyl acetate>tetrahydrofuran. Binary mixtures were also used: hexane/2-propanol 90/10 (v/v) and ethyl acetate/2-propanol 25/75, 50/50 and 75/25 (v/v) In general, protic solvents showed higher initial hydrogenation rates compared to aprotic polar solvents [II].

The reactant conversion was above 90 % in all the solvents except tetrahydrofuran (THF) where it was below 30 %. THF is known to have a strong interaction with the catalyst surface due to oxygen lone pair orbital bonding (Augustine, 1984; Sexton, 1984). The competition of the solvent and the reactant could explain a low initial hydrogenation rate and reactant conversion obtained in THF.

### 3.10.2 Enantioselectivity

The enantiomeric excess in the hydrogenation of ethyl benzoylformate depends on the solvent properties. The highest ee was obtained in ethyl acetate while the lowest one was observed in ethanol [III]. In general, aprotic polar solvents gave higher enantiomeric excess compared to protic solvents (Fig. 20).

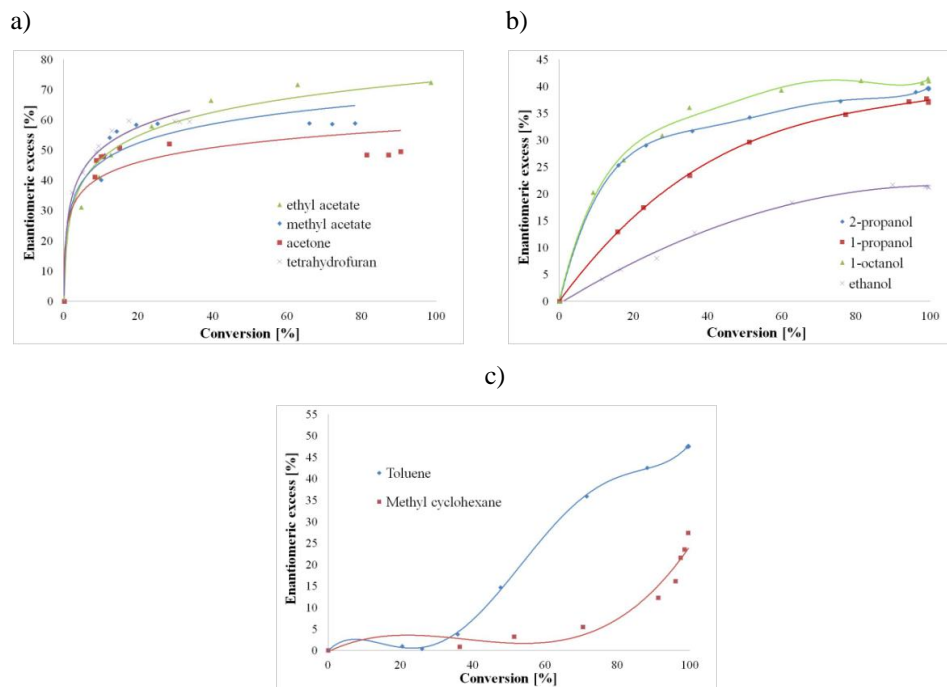


**Figure 20.** Relation between enantiomeric excess and reactant conversion for a) aprotic b) protic and c) non-polar solvents. Reaction conditions: 0.85 mmol of ethyl benzoylformate, 0.16 n(CD) / n(Surface Pt), 220 mg of 5 wt% Pt/Al<sub>2</sub>O<sub>3</sub> (<90 μm), 150 mL of solvent, 25 °C and p<sub>H<sub>2</sub></sub> = 1.

### 3.10.3 Influence of ethyl acetate and 2-propanol mixtures

The influence of binary solvent mixtures using ethyl acetate and 2-propanol was studied. The dielectric constant range varied from 6.2 (ethyl acetate) to 18.3 (2-propanol). The dependence of ee on the dielectric constant is illustrated in Fig. 21. The initial hydrogenation rates in solvent mixtures varied between the boundary values observed in

pure ethyl acetate and 2-propanol and the ee decreased with increasing dielectric constant [II].

It should be noted that although solvent mixtures allow a reliable investigation of dielectric constant influence on ee, the selection of solvents for a binary or ternary mixture should be done carefully in order to avoid chemical reactions between the solvents and the catalyst.

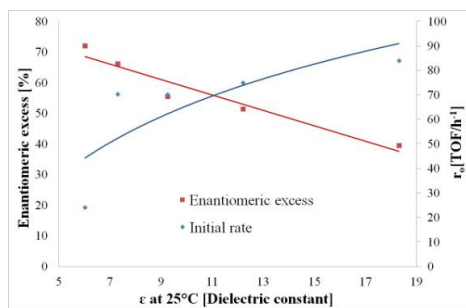


**Figure 21.** Influence of binary solvent mixture on the enantioselective hydrogenation of ethyl benzoylformate. Reaction conditions: 0.85 mmol of ethyl benzoylformate, 0.16 n (CD) / n (Surface Pt), 220 mg of 5 wt% Pt/Al<sub>2</sub>O<sub>3</sub> (<90 μm), 150 mL of solvent, 25 °C and  $p_{H_2} = 1$ .

### 3.11 DFT results

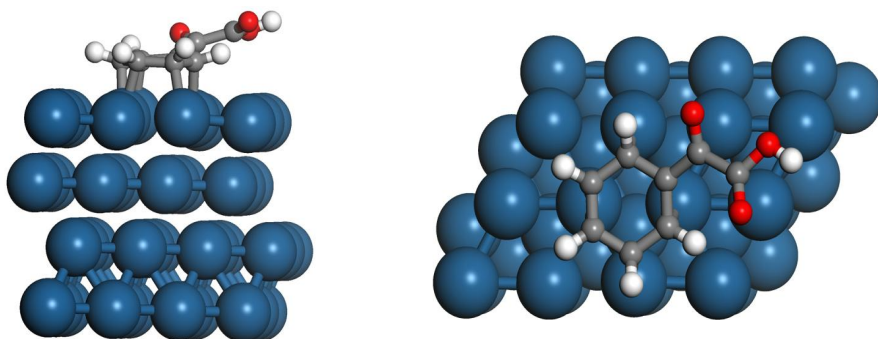
The adsorption of ethyl benzoylformate was investigated on the platinum surface. The adsorption energies for five different geometries were calculated (Table 6). Figure 22 shows different geometries calculated and the best one corresponds to geometry number 4 (Table 6). Geometry number 5 differs only slightly in a way that OH-group points towards the surface. Negative values refer to exothermic adsorption.

DFT calculations allowed to restrain the number of sites occupied by EBF on the catalyst to a specific range, i.e. 9-11.

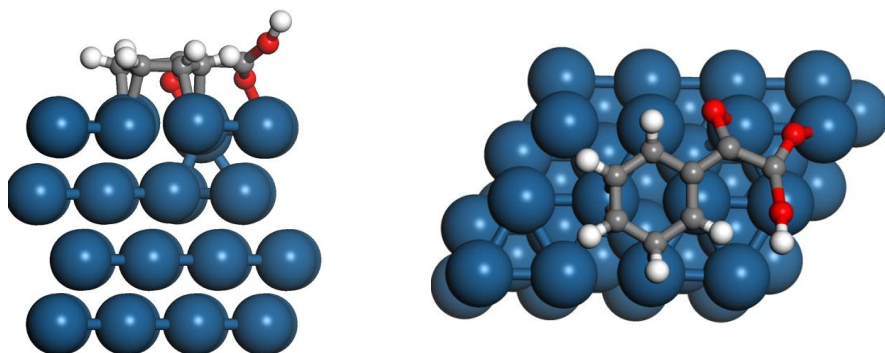
**Table 6.** Adsorption energies for different geometries of ethyl benzoylformate over Pt(1 1 1).

<i>Geometry</i>	<i>Adsorption energy (KJ/mol)</i>
1	30.26
2	-14.4
3	-25.1
4	-50.4
5	-46.3

a)



b)



c)

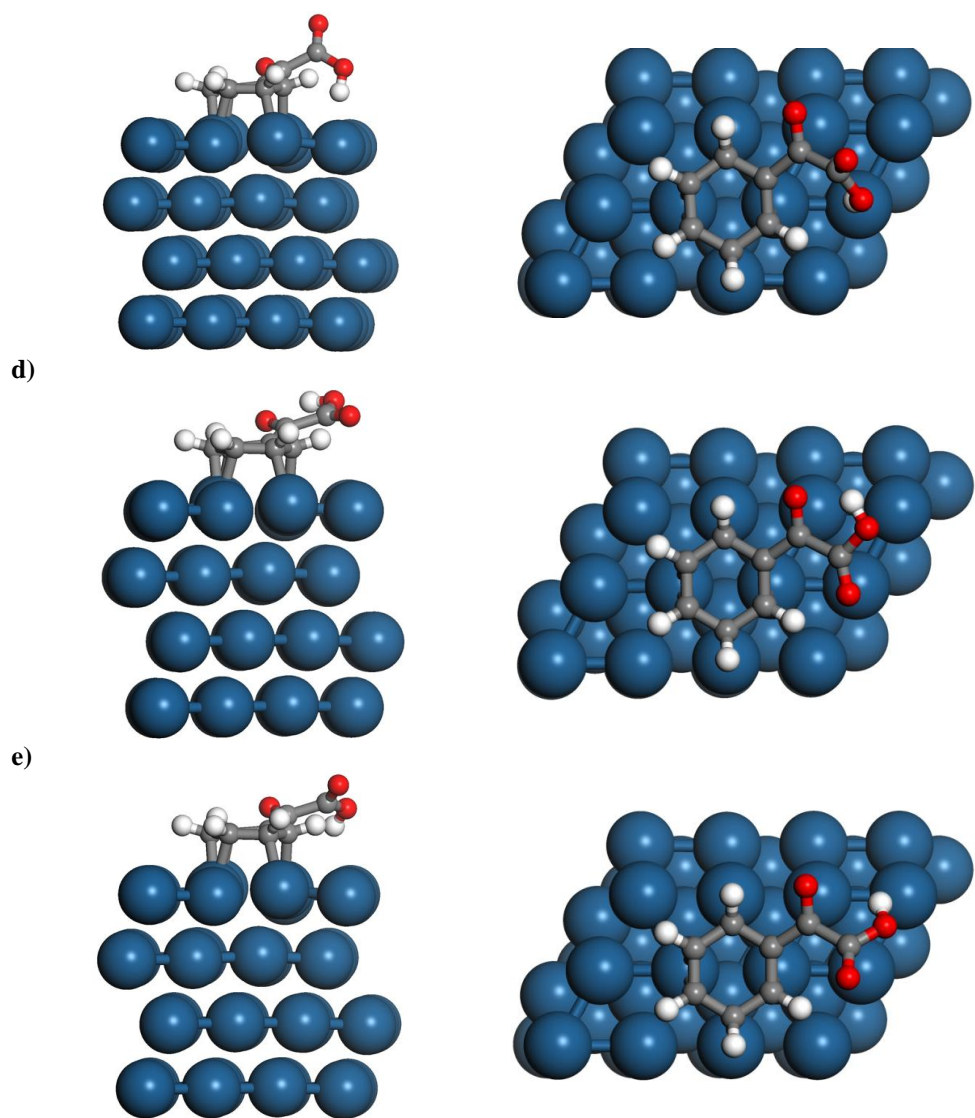


**Figure 22.** The adsorption geometries for ethyl benzoylformate on the Pt(1 1 1) surface. Carbon atoms are colored grey, hydrogen atoms white, oxygen atoms red and platinum atoms blue.

## 3.12 Modeling results

### 3.12.1 Hydrogenation rates

The quantitative treatment of the hydrogenation kinetics is based on the reaction scheme displayed in Fig. 23. Two adsorption modes of the modifier were selected for modeling, one mode being the parallel adsorbed species of (-)-cinchonidine involved in the enantiodifferentiation and the other being adsorbed in tilted mode only as a spectator on the catalyst surface (Fig. 24). Open and closed conformers of (-)-cinchonidine were not taken into account; however, it can be expected that the closed conformer also adsorbs in somewhat similar fashion and the steric constraints are similar to the open conformer. The conformation equilibrium of (-)-cinchonidine is influenced by the choice of solvent (Martin, 2013) and therefore, the varying conformational equilibria (open, closed) were left outside of the current work, as only toluene was used as a solvent.

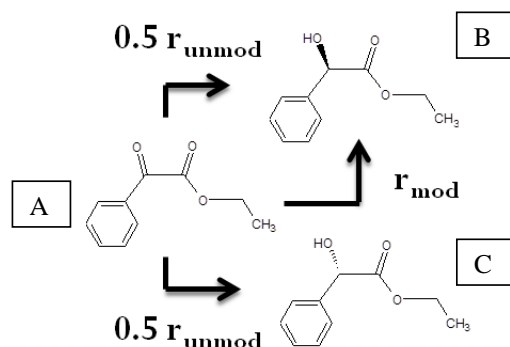


**Figure 23.** Schematic representation of the reaction network (Toukoniitty E, 2010).

The adsorption steps of the organic compounds are assumed to be rapid compared to the hydrogenation steps, which implies that quasi-equilibria are applied to the adsorption steps of the reactant (A) as well as the modifier (M). The adsorption of the product molecules is neglected. Only the hydrogenation steps to B and C (Fig 2) are considered here, since none of the diols formation was observed during the experiments. For similar reasons the phenyl ring hydrogenation is discarded. The hydrogenation steps are presumed to be irreversible and determine the rate of product formation. Finally, the product-modifier

interactions were not taken into account because the chemistry of such interactions is unclear and multisite adsorption was sufficient.

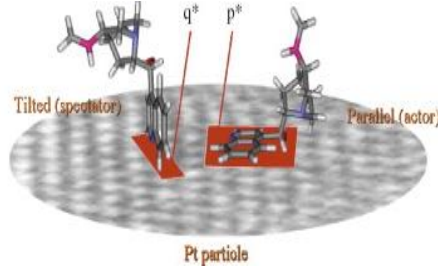


**Figure 24.** Different adsorption modes of the modifier (M) on Pt surface.

A more detailed account of the derivation of the model as well as details about the general methods employed for the parameter estimation of the aforementioned model are presented in [III]

Reaction rate equations acquire their final forms after inserting the surface concentrations of hydrogen. For practical purposes, the rate expressions are compressed to

$$r_{unmod} = r_5 = k'_5 \left( \frac{\sqrt{K_{H_2} C_{H_2}}}{1 + \sqrt{K_{H_2} C_{H_2}}} \right)^2 C_A \Theta^m \quad (3)$$

$$r_{mod} = r_7 = k'_7 \left( \frac{\sqrt{K_{H_2} C_{H_2}}}{1 + \sqrt{K_{H_2} C_{H_2}}} \right)^2 C_A C_M \Theta^{m+p+f} \quad (4)$$

where the combined parameters ( $k'$ ) contain the rate constants ( $k$ ), the equilibrium constants ( $K$ ), and the total concentration of sites ( $c_0$ ).

### 3.12.2 Components generation rates and mass balances

The generation rates of the compounds are obtained from the stoichiometric scheme (Fig 23).

$$r_A = -r_{unmod} - r_{mod} \quad (5)$$

$$r_B = 0.5r_{unmod} + r_{mod} \quad (6)$$

$$r_C = 0.5r_{unmod} \quad (7)$$

The generation rates are combined with the mass balances of the components [III]. The balance equations of the organic components become

$$d_{Ci}/d_t = \rho_B r_i \quad (8)$$

where  $i = \text{EBF}, (R)\text{- or } (S)\text{-ethyl mandelate}$  and  $\rho_B$  is the mass-of-catalyst-to-liquid-volume ratio.

### 3.12.3 Parameter estimation procedure

For parameter estimation purposes primary concentration vs time data from 8 experiments were used. The fraction of vacant sites ( $\theta$ ) was calculated during the estimation. A detailed description is presented in [III].

The residual sum of squares (Q) was minimized during the parameter estimation,

$$Q = \sum (C_{i,t(model)} - C_{i,t(exp)})^2 \quad (9)$$

where the subscripts  $i$  and  $t$  refer to components and the corresponding times, respectively. The model predictions were obtained by solving the differential equation system (8) (ODEs) for all of the components (EBF, (R)- and (S)-ethyl mandelate) during the parameter estimation. The residual sum of squares was minimized by a combined Simplex–Levenberg–Marquardt algorithm implemented in the software Modest (Haario, 2001).

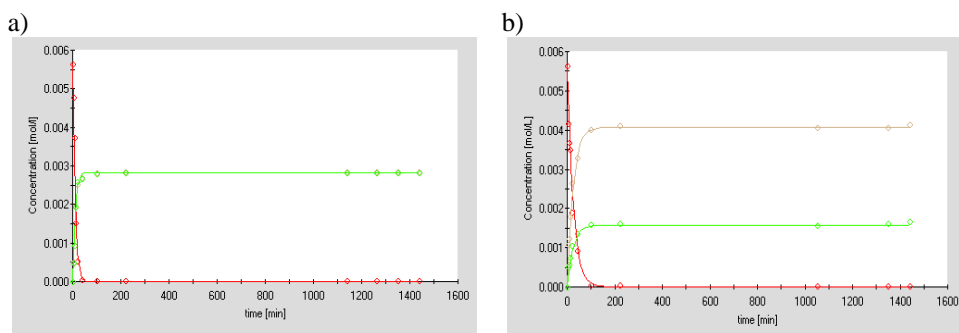
### 3.12.4 Results from parameter estimation

The results from the model simulation presented in Table 7 showed good statistics for the estimated parameters. The degree of explanation obtained by the model was 96 %, which indicates very good prediction for the concentration of the reactant and products (Fig. 25).

**Table 7.** Kinetic and adsorption parameters obtained from parameter regression. Degree of explanation 96 %

<i>Parameter</i>	<i>Value</i>	<i>Units</i>	<i>Relative error %</i>
m	9.4		48
p	16.8		48
q	3.5		47
f	0		0
$K'_1$	8.9	L mol <sup>-1</sup>	46
$K'_2$	1.34x10 <sup>5</sup>	L mol <sup>-1</sup>	52
$K'_3$	3.50x10 <sup>3</sup>	L mol <sup>-1</sup>	43
$K'_4$	13.1	L <sup>2</sup> mol <sup>-2</sup>	Large
$K_H$	4.48x10 <sup>-4</sup>	1 atm <sup>-1</sup>	30
$k'_5$	1.96x10 <sup>2</sup>	L s <sup>-1</sup> g <sub>cat</sub> <sup>-1</sup>	28
$k'_7$	1.66x10 <sup>8</sup>	L <sup>2</sup> s <sup>-1</sup> g <sub>cat</sub> <sup>-1</sup>	29

Besides the overall applicability of the model illustrated in Figure 25, the kinetic model also predicted observed kinetic regularities, such as concentration dependence on hydrogen pressure (Fig. 26). The independence of enantioselectivity on hydrogen pressure was also followed by the model (Fig. 27).



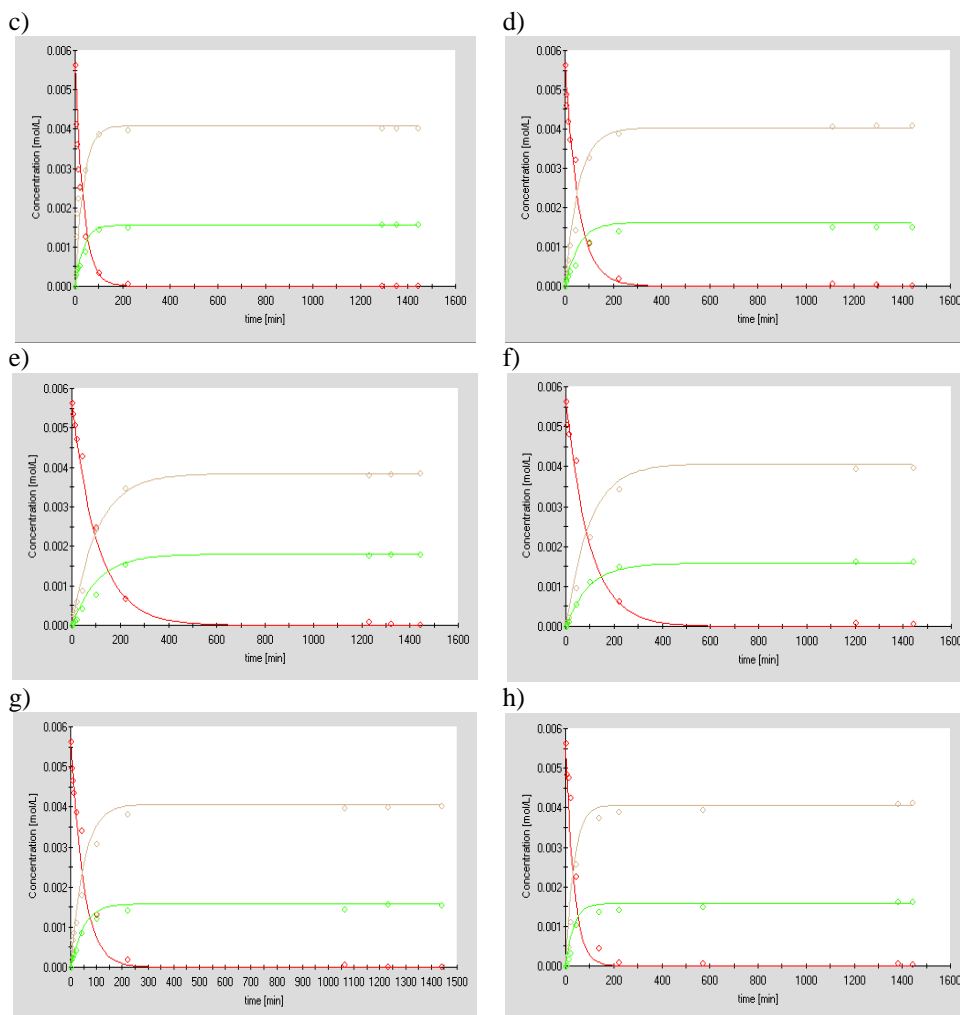


**Figure 25.** Model prediction for the hydrogenation of ethyl benzoylformate. Points: experimental; line: calculated. Reaction conditions: 0.85 mmol of ethyl benzoylformate, 220 mg of 5 wt% Pt/Al<sub>2</sub>O<sub>3</sub> (<90 μm), 150 mL of toluene and 25 °C

- |   |  |
|---|--|
| a) [CD]=0 mmol/L and p <sub>H<sub>2</sub></sub> = 1 atm     | e) [CD]=0.16 mmol/L and p <sub>H<sub>2</sub></sub> = 1 atm     |
| b) [CD]=0.020 mmol/L and p <sub>H<sub>2</sub></sub> = 1 atm | f) [CD]=0.020 mmol/L and p <sub>H<sub>2</sub></sub> = 0.25 atm |
| c) [CD]=0.041 mmol/L and p <sub>H<sub>2</sub></sub> = 1 atm | g) [CD]=0.020 mmol/L and p <sub>H<sub>2</sub></sub> = 0.5 atm  |
| d) [CD]=0.081 mmol/L and p <sub>H<sub>2</sub></sub> = 1 atm | h) [CD]=0.020mmol/L and p <sub>H<sub>2</sub></sub> = 0.75 atm  |

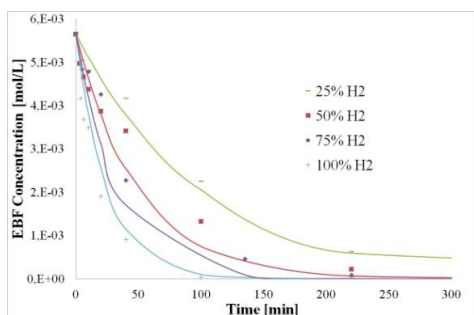


**Figure 26.** Model prediction for the hydrogenation of ethyl benzoylformate at different pressures. Points: experimental; line: calculated. Reaction conditions: See **Figure 25**

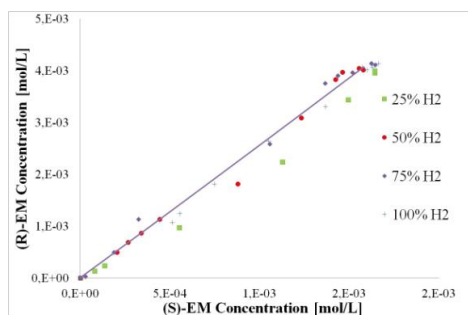


**Figure 27.** Model prediction for the enantioselectivity at different hydrogen pressures. Points: experimental; line: calculated. Reaction conditions: See **Figure 25**

Analogously, the developed kinetic model can correctly capture dependences of the rate on the modifier concentration (Fig. 28), as well as the increase of ee with conversion (Fig. 29).

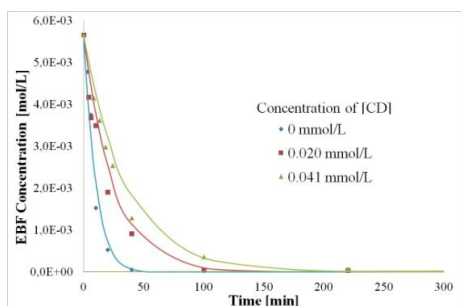


**Figure 28.** Model prediction for the hydrogenation of ethyl benzoylformate at different modifier amounts. Points: experimental; line: calculated. Reaction conditions: See **Figure 25**

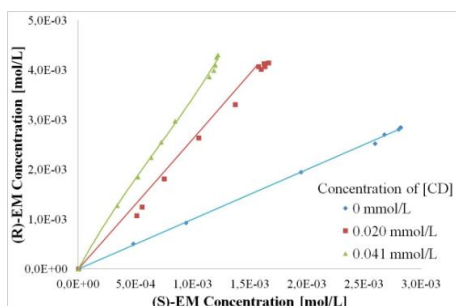


**Figure 29.** Model prediction for the hydrogenation of ethyl benzoylformate at different modifier amounts. Points: experimental; line: calculated. Reaction conditions: See **Figure 25**

### 3.12.5 Solvent effect extension

The target in the modeling was to include the solvent effects on the catalytic hydrogenation. For this reason, the transition state theory was used as a tool to get a better understanding of the reaction path. Keeping in mind that the enantio-differentiating transition state includes both the reactant and the modifier, it can be treated as a dipole–

dipole interaction. The Kirkwood treatment (Laidler, 1987) for the case when the reactants are not charged leads to

$$\ln k_{\text{mod}} = \ln k_{\text{mod}}^0 - k'' \frac{(\mu^\ddagger)^2 - (\mu_A)^2 - (\mu_B)^2 - (\mu_M)^2}{\varepsilon};$$

$$\ln k_{\text{umod}} = \ln k_{\text{umod}}^0 - k''' \frac{(\mu^\ddagger)^2 - (\mu_A)^2}{\varepsilon}$$
(10)

where  $\varepsilon$  is the dielectric constant,  $\mu$  denotes the dipole moments and  $k''$  and  $k'''$  are temperature dependent constants.

A more detailed description of the derivation of the model as well as details about the general methods employed for the parameter estimation of the aforementioned extension are presented in [II]

The end-of-experiment values of enantioselectivity are thus given as:

$$eS = \frac{1 + \beta_B e^{a_B/\varepsilon}}{1 + \beta_C e^{a_C/\varepsilon}}$$
(11)

where

$$\beta_B = 2 \frac{k_{B,\text{mod}}^0}{k_{\text{umod}}^0} C_M C_B^{\text{final}}, \quad \beta_C = 2 \frac{k_{C,\text{mod}}^0}{k_{\text{umod}}^0} C_M C_C^{\text{final}}$$
(12)

$$\alpha_B = \alpha_{2B} - \alpha_1, \quad \alpha_C = \alpha_{2C} - \alpha_1$$

Eq. (11) was used to describe the dependence of enantioselectivity values at full conversion as a function of the dielectric constant (Fig. 30). The model was able to describe the main trend with reasonable accuracy although the values of parameter  $\beta$  are not well defined.

The results of the calculations demonstrated, that the model fitted the experimental data very well. Some outliers were presented in the experimental data such as the  $ee$  showed by 1-octanol and acetone. These were not taken into consideration for the calculations.

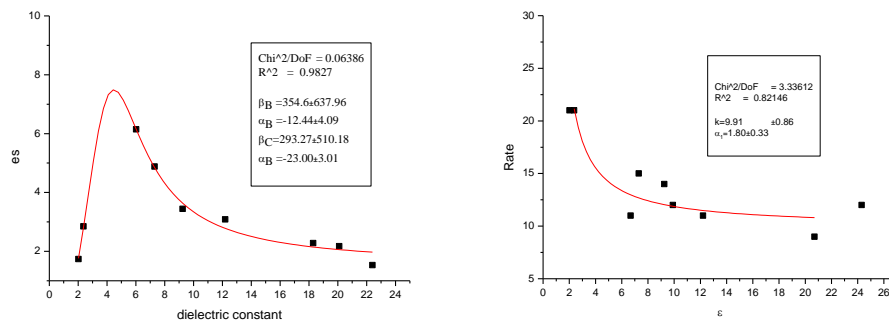


**Figure 30.** Dependence of **Figure 31.** Dependence of the initial enantioselectivity on the solvent dielectric reaction rates on the solvent dielectric constant. Points: experimental; line: constant. Points: experimental; line: calculated

The impact of solvent polarity on the hydrogenation rate could be evaluated and since the initial hydrogenation was almost racemic, the initial hydrogenation rate is expressed by

$$r = ke^{\alpha_1/\epsilon} \quad (13)$$

According to Eq (13), the reaction rate decreases with increasing solvent dielectric constant, if hydrogen solubility is taken as constant. The binary mixture hexane/2-propanol 90/10 (v/v) was not taken into account in the model. However, the results presented by this solvent were similar to the one obtained with toluene for the enantioselectivity and initial reaction rate. The exceptions were ethyl acetate and tetrahydrofuran and protic solvents such as 1- and 2-propanol [II]. Without these solvents the model (13) correctly captured the main trend in the dependence of the initial rates on solvent polarity (Figure 31).

### 3.13 Continuous hydrogenation

The enantioselective hydrogenation of ethyl benzoylformate (EBF) over (-)-cinchonidine (CD)-modified Pt/Al<sub>2</sub>O<sub>3</sub> catalyst in a continuous fixed bed reactor was studied. Hexane/2-propanol 90/10 (v/v) was used as solvent in all the experiments. The modifier concentration and reaction temperature were the main parameters. The typical hydrogenation kinetics of ethyl benzoylformate is shown in Fig. 32. The residence time

distribution was measured with tracer experiments and the hydrogenation was studied with transient experiments [IV].

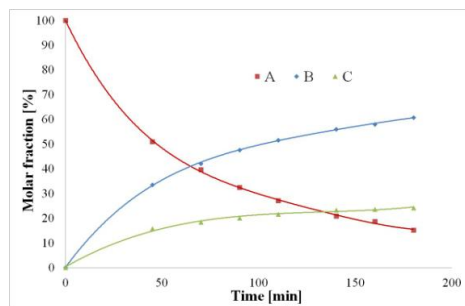


**Figure 32.** The hydrogenation kinetics of EBF (A) in the fixed-bed reactor. Experiment conditions: EBF concentration  $5.6 \text{ mmol L}^{-1}$ , 61 g of 1 wt% Pt/ $\text{Al}_2\text{O}_3$  (3.2 mm pellets), 0.16 n (CD) / n (Surface Pt), flow rate  $5 \text{ mL min}^{-1}$ ,  $25 \text{ }^\circ\text{C}$ ,  $\text{pH}_2 = 1 \text{ atm}$ .

### 3.13.1 Residence time distribution

The result from the residence time distribution is presented in Fig. 33. The steady state was achieved after 100 min of continuous flowing.

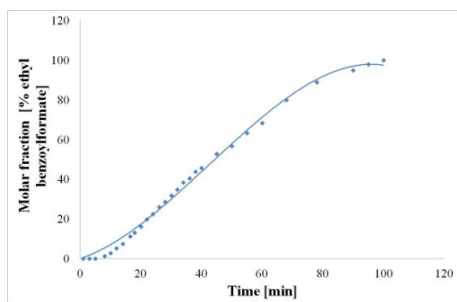


**Figure 33.** Residence time distribution for ethyl benzoylformate in the fixed-bed reactor. Experiment conditions: EBF concentration  $5.6 \text{ mmol L}^{-1}$ , 61 g of 1 wt% Pt/ $\text{Al}_2\text{O}_3$  (3.2 mm pellets), flow rate  $5 \text{ mL min}^{-1}$ ,  $25 \text{ }^\circ\text{C}$ ,  $\text{pH}_2 = 1 \text{ atm}$ .

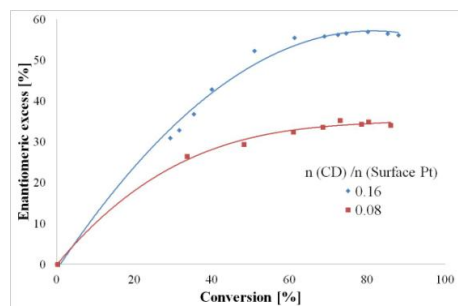


**Figure 34.** Influence of the mass of modifier in the continuous reactor. Reaction conditions: EBF concentration  $5.6 \text{ mmol L}^{-1}$ , 61 g of 1 wt% Pt/ $\text{Al}_2\text{O}_3$  (3.2 mm pellets), flow rate  $5 \text{ mL min}^{-1}$ ,  $25 \text{ }^\circ\text{C}$ ,  $\text{pH}_2 = 1 \text{ atm}$ .

### 3.13.2 Dependence on the (-)-cinchonidine concentration

The highest ee achieved was 57 % in a 200 min reaction time (Fig. 34). In this continuous reactor, when the amount of the modifier increased from 0.08 to 0.16 (mol CD/mol surface Pt) the steady state moved from 50 % to 65% conversion. However, the relative low modifier concentration used in the experiments affected mainly the product selectivity and not to considerable extent the catalyst activity [IV].

### 3.13.3 Transient experiments

Transient experiments were carried out in the continuous fixed bed reactor. The initial transient period of the enantioselectivity was shorter with a shorter residence time (Fig. 36). As the liquid flow rate was higher, the steady-state enantioselectivity was achieved more rapidly.

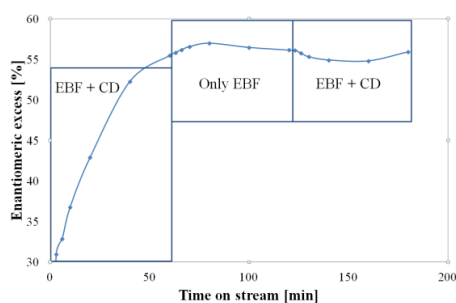


**Figure 35.** Influence of modifier pulses in the continuous reactor. Reaction conditions: EBF concentration  $5.6 \text{ mmol L}^{-1}$ , 61 g of 1 wt% Pt/ $\text{Al}_2\text{O}_3$  (3.2 mm pellets), flow rate  $5 \text{ mL min}^{-1}$ ,  $25 \text{ }^\circ\text{C}$ ,  $\text{pH}_2 = 1 \text{ atm}$ .

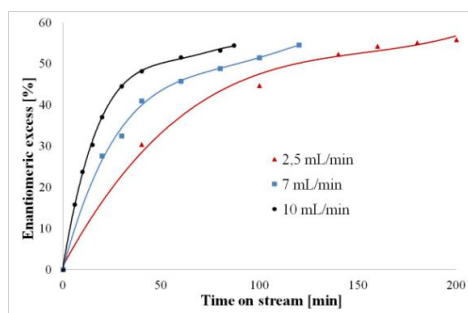


**Figure 36.** Influence of the flow rates in the continuous reactor. Reaction conditions: EBF concentration  $5.6 \text{ mmol L}^{-1}$ , 61 g of 1 wt% Pt/ $\text{Al}_2\text{O}_3$  (3.2 mm pellets),  $0.16 \text{ n (CD) / n (Surface Pt)}$ ,  $25 \text{ }^\circ\text{C}$  and  $\text{pH}_2 = 1 \text{ atm}$ .

In the second experiment, both reactant and modifiers were fed into the reactor simultaneously. After 60 min of time-on-stream the modifier feed was stopped and then at 120 min of time-on-stream the modifier feed was re-started (Fig. 35). The results showed that continuous feeding of modifier is needed in order to keep a high steady state ee [IV].

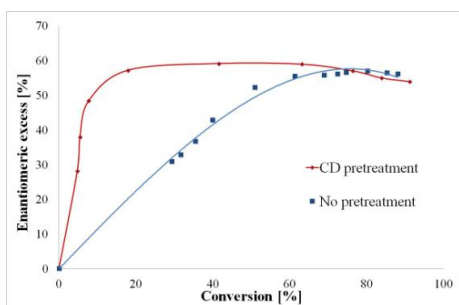


**Figure 37.** Influence of modifier pretreatment in the continuous reactor. Reaction conditions: See **Figure 32**. In the pretreatment, solvent and modifier were fed into the reactor for 60 min prior to the raw material injection.

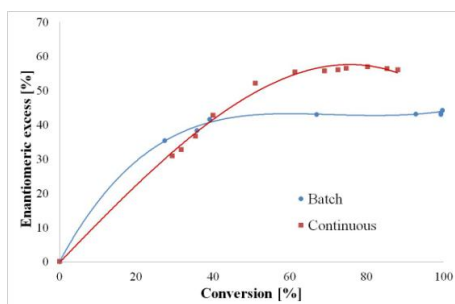


**Figure 38.** A comparison of the enantiomeric excess in the semi-batch and continuous reactor. Reaction conditions: See **Figure 32** for continuous and **Figure 11** for batch reactor. The modifier-to-surface Pt ratio used in both experiments was 0.16

In the third experiment, a pretreatment of the catalyst was made to ensure that the modifier was evenly distributed on the catalyst surface. The enantiomeric excess increased to steady state before reaching 20 % conversion. However, a decrease in ee due to the desorption of modifier took place at 80 % conversion which in this case was expected [IV].

In order to compare the enantiomeric excesses in the batch and continuous reactors (Fig. 38), productivity for both cases was calculated at 200 min reaction time. The ratio estimated in this case corresponds to the amount determined in the batch system (0.16). However, the mol of CD passing through the continuous reactor in 3 hours was equivalent to the ratio estimated in the batch system. The productivity was  $0.044 \text{ mmol min}^{-1} \text{ g}_{\text{Pt}}^{-1}$  and  $0.35 \text{ mmol min}^{-1} \text{ g}_{\text{Pt}}^{-1}$  for respectively continuous and batch reactors. A plausible explanation for the higher productivity in the batch compared to the continuous system could be the vigorous stirring present in the batch reactor while the data in the former are influenced by mass transfer.

### 3.14 Chromatographic separation

#### 3.14.1 Adsorption of modifier by tris-[3,5-dimethylphenyl] carbamoyl cellulose

In order to determine the capability of tris-[3,5-dimethylphenyl] carbamoyl cellulose to adsorb (-)-cinchonidine, UV measurements were done before and after the injections. Huck et. al. have found that the UV spectrum showed broad bands at around 305 and 318 nm, which belong to modifiers (-)-cinchonidine (CD) and quinidine (QD), respectively, possessing a partially hydrogenated quinoline ring system (Huck, 2003). Two different concentrations of modifier were applied  $[CD] = 0.08$  and  $0.02$  mmol/L and the results are presented in Fig. 39.

Both concentrations were tested in duplicate. Lines 1 and 2 represent  $[CD] = 0.02$  mmol/L while 3 and 4 at  $0.08$  mmol/L. The results showed that the modifier adsorption was complete not being present at the outlet.

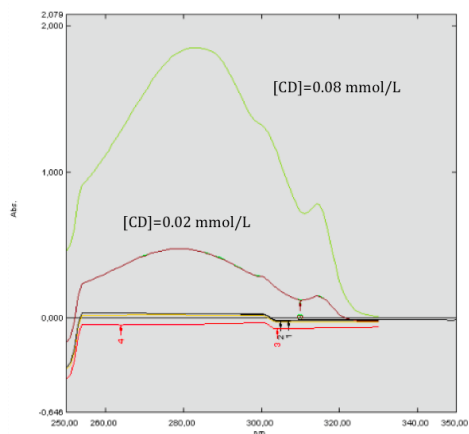


**Figure 39.** UV spectrum for the adsorption of (-)-cinchonidine on tris-[3,5-dimethylphenyl] carbamoyl cellulose

#### 3.14.2 Pulses and breakthrough experiments

During the determination of the single component adsorption equilibrium isotherms by preparative pulse experiments, the injection volume was  $100 \mu\text{L}$ . Injections were made

at least in duplicate. The concentration ranges of the enantiomers were set to reflect its typical content in the post-reaction mixture. The feed concentration ranges were as follows:

- TTBB: 0.5, 4.65 and 9.3 g/L
- (*R*)-ethyl mandelate: 0.5, 4.65 and 9.3 g/L
- (*S*)-ethyl mandelate: 0.5, 4.65 and 9.3 g/L
- Outlet concentration from the continuous reactor ([B]=0.74g/L and [C]=0.21 g/L)

The first statistical moments were used to obtain the retention times,  $t_R$ , for each pulse experiment Eq. (14),

$$t_R = \frac{\int_0^{\infty} tC(t)dt}{\int_0^{\infty} C(t)} \quad (14)$$

The obtained retention times of the enantiomers were independent of the feed concentration. Therefore, the adsorption equilibrium constants (distribution coefficients),  $K_i$ , of the linear isotherms were proportional to the retention times and they were calculated from the following equation:

$$t_R = \frac{\varepsilon V_C}{Q} \left( 1 + \frac{1 - \varepsilon}{\varepsilon} K_i \right) \quad (15)$$

where  $\varepsilon$  is the bulk porosity,  $K_i$  is the distribution coefficient of the component  $i$ ,  $V_C$  is the bed volume and  $Q$  is the volumetric flow rate (Rabelo, 2013).

The concentrations at the column outlet were measured online by the UV detector at 270 nm. The stoichiometric time calculated from one experimental breakthrough curve is given by eq. 15. For linear systems, it is equal to the retention time calculated from pulse experiments.

The plot of the reciprocal value of the retention time as a function of flow rate is shown in Fig. 40. The bulk porosity ( $\varepsilon$ ) was determined from the slope of the straight-line plot giving a value of 0.49.

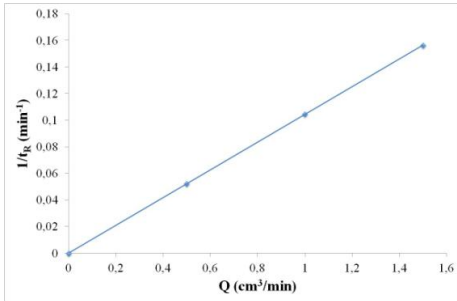


**Figure 40.** Reciprocal retention time ( $1/t_R$ ) vs. flow rate ( $Q$ ) for 1,3,5-tri-tert-butylbenzene.

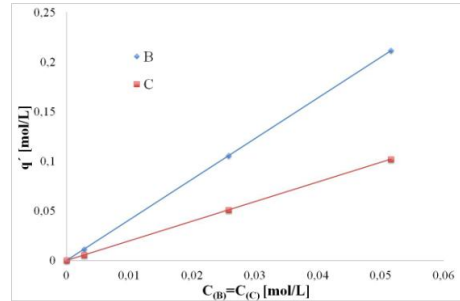


**Figure 41.** Adsorption equilibrium isotherms of (*R*)-ethyl mandelate (◆) and (*S*)-ethyl mandelate (■) on tris-[3,5-dimethylphenyl] carbamoyl cellulose at 25°C.

The distribution coefficients ( $K_i$ ) were calculated according to eq. (15) for three different feed concentrations. Their values for both enantiomers did not change with the concentration which confirmed a very good linearity of the adsorption isotherms (Fig. 41). The experimental values were determined by regression analysis and the adsorption constants obtained for  $K_R$  and  $K_S$  were 4.09 and 1.98, respectively.

### 3.14.3 Mathematical model

A dispersive plug flow model was used to fit the experimental elution profiles and breakthrough curves of individual enantiomers. Several assumptions were included in this model: isothermal adsorption, axial dispersion flow, constant flow rate, constant porosity and no radial gradient within the bed (Luz, 2008). The mass balance equation of an adsorbing component can be written as:

$$\frac{\partial C_i}{\partial t} + \frac{(1-\varepsilon)}{\varepsilon} \frac{\partial \bar{q}_i}{\partial t} + u_{int} \frac{\partial C_i}{\partial z} - D_a \frac{\partial^2 C_i}{\partial z^2} = 0 \quad (16)$$

where  $C_i$  and  $\bar{q}_i$  are the liquid-phase and average adsorbed solid-phase concentrations of the  $i$ th species, respectively;  $u_{int}$  is the interstitial velocity,  $D_a$  is the axial dispersion coefficient; the variables  $t$  and  $z$  refer to the time and axial coordinates, respectively.

A more detailed description of the derivation of the model as well as details about the general methods employed for the parameter estimation of the aforementioned model are presented in article [V].

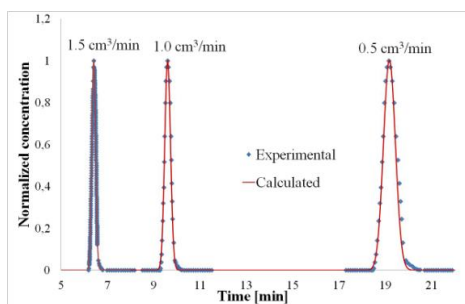


**Figure 42.** Experimental (*points*) and simulated elution profiles (*solid lines*) of TTBB at different flow rates (0.5, 1.0 and 1.5 cm<sup>3</sup>/min) obtained in single-component pulse experiments at 25 °C.

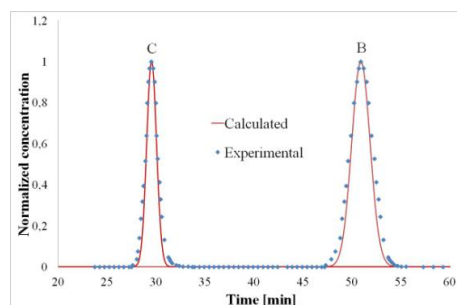


**Figure 43.** Experimental (*points*) and simulated elution profiles (*solid lines*) of (R)- and (S)-ethyl mandelate at 4.65 g/L obtained in single-component pulse experiments at 25 °C.

The validity of the mathematical model was checked for different pulse and breakthrough experiments. Figures 41, 42 and 43 were obtained using the data in Table 8. These experiments were carried out at a flow rate of 1.0 cm<sup>3</sup>/min and at a temperature of 25°C.

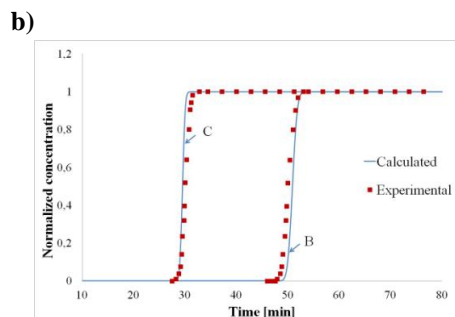
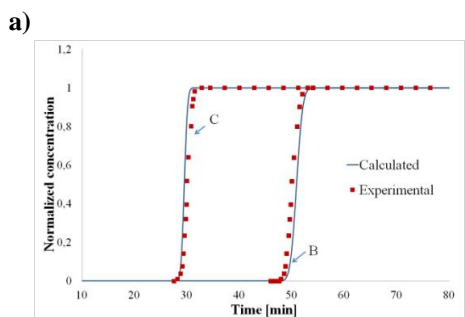


**Figure 44.** Experimental (*points*) and simulated (*solid lines*) breakthrough curves of (R)- and (S)-ethyl mandelate at different concentrations (a) 4.65 g/L and (b) outlet concentration from the continuous reactor ([B]=0.74g/L and [C]=0.21 g/L) at 25 °C.

Experimental and simulated results for pulses of unretained species (TTBB) are displayed in Fig. 42. Different flow rates were used including 0.5, 1.0 and 1.5 cm<sup>3</sup>/min. The simulated elution profiles showed a very good agreement to the experimental values.

Additionally, single pulses of both enantiomers were injected and one of the results is shown in Fig. 43. The first peak corresponds to the less strongly adsorbed enantiomer ((*S*)-ethyl mandelate, C), while the second peak to the stronger adsorbed enantiomer ((*R*)-ethyl mandelate, B). The experimental data were very well predicted by the model.

Single-component breakthrough curves were also simulated and one of the results is shown in Fig. 44. The proposed model with the used parameters described the experimental data very well throughout the entire concentration range.

It can be concluded that preparative pulse experiments of single-component solutions provided reliable values of adsorption isotherm parameters of (*R*)- and (*S*)- ethyl mandelates on tris-[3,5-dimethylphenyl] carbamoyl cellulose resins up to moderately high concentrations.

**Table 8.** Parameters used in the mathematical model

<i>Parameters</i>	<i>Kromasil</i> $d_p=10 \mu m$
$Q$ [cm <sup>3</sup> /min]	1.0
$d_p$ [μm]	5.6
$L$ [cm]	25.0
$\varepsilon_T$	0.67
$\varepsilon$	0.49
$\varepsilon_p$	0.35
$Pe$	12500
$D_m$ [cm <sup>2</sup> /s]	$2.2 \times 10^{-5}$
$\tau_p$	7.8
$\rho$ [g/mL]	0.6
$k_{h,B}$ [s <sup>-1</sup> ]	0.39
$k_{h,C}$ [s <sup>-1</sup> ]	0.19
$MW_i$ [g/mol]	180.2
$Vmol_i$ [cm <sup>3</sup> /mol]	214
$Vmol_S$ [cm <sup>3</sup> /mol]	131.1
$\eta_S$ [cP]	0.48

#### 3.14.4 Simulated moving bed operating conditions

With the adsorption isotherms for the (*R*)- and (*S*)-ethyl mandelate, it was possible to identify the window of operating conditions that allowed a complete separation of the components. This window is delimited by constraints imposed on the velocity ratios ( $\gamma_i$ ) between mobile (liquid) and stationary (solid) phases in the different zones, considering the equivalent representation of a true moving bed. These constraints are given by equations (17-19):

$$\gamma_1 > vK_B \quad (17)$$

$$vK_C < \gamma_2 < \gamma_3 < vK_B \quad (18)$$

$$\gamma_4 < vK_C \quad (19)$$

where the subscript B refers to the strongest adsorbed ((*R*)-ethyl mandelate) component and C refers to the least adsorbed ((*S*)-ethyl mandelate) for a binary separation. The parameter  $v$  is the solid/liquid phase ratio ( $1/\varepsilon - 1$ ). B and C would be separated in a way that the product extract would contain all (*R*)- and the raffinate would contain the (*S*)-ethyl mandelate or vice-versa

The region, as given by the equilibrium theory, is shown in Fig. 45. The vertex of each of the triangles indicates the optimal condition under which complete separation is still possible (neglecting mass transfer effects).

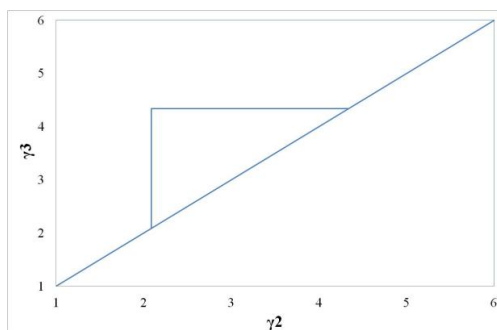


**Figure 45.** Region of complete separation of a simulated moving bed, according to the equilibrium theory. Parameters  $\gamma_2$  and  $\gamma_3$  are fluid-solid velocity ratios in sections 2 and 3 of an equivalent true moving bed. Complete separation is defined as the collection of 100% pure (*R*)-ethyl mandelate in the raffinate product and 100% pure (*S*)-ethyl mandelate in the extract product.

Finally, the SMB is a promising technology for the separation of enantiomers. Future studies should focus on determining the real region of complete separation and the switching time for different column configurations.

### 3.15 Racemization results

After 24 hours of reaction, less than 5 % conversion of (*S*)-ethyl mandelate to (*R*)-ethyl mandelate was observed. Higher temperatures and pressures could be an alternative, however, strong condition could lead to decomposition or cracking of the reactant.

## 4 CONCLUSIONS

Enantioselective hydrogenation of ethyl benzoylformate in toluene was investigated in a batch reactor at atmospheric pressure on a finely dispersed Pt/Al<sub>2</sub>O<sub>3</sub> catalyst. External and internal mass transfer limitations were overcome by high stirring rate and small particle size, respectively. The effect of temperature on enantioselectivity was strong with high temperature (>50°C) leading to desorption of the modifier, therefore, low temperatures (<25°C) were preferred. Catalyst deactivation by sulfur and fluorine from the feedstock was observed, however, application of activated carbon proved to be sufficient for removal of all poisoning agents. Hydrogen did not influence the enantioselectivity, whereas a large influence on the initial hydrogenation rate was observed.

The (-)-cinchonidine amount was a key factor in the enantiodifferentiation. The initial hydrogenation rate and enantioselectivity increased as the amount of modifier increased up to a maximum. After this, a further increase leads to a decrease in both values due to competitive adsorption between the reactant and the modifier.

The solvent nature showed a strong influence on the enantiomeric excess and the initial hydrogenation rate. For the former, the ee increased up to a maximum and then started decreasing as the dielectric coefficient increased. For the second, the initial rate showed to decrease as the dielectric coefficient increased.

The solvent effect was included in an advanced kinetic model in order to describe quantitatively the variation of the enantioselectivity in different solvents. The dielectric constant dependence was taken into consideration by applying the transition state theory and the Kirkwood treatment, which accounts for the effects of the solvent dielectric constant on the rate constant. A good description of the rates and enantioselectivity was obtained.

A kinetic model was developed for the enantioselective hydrogenation of ethyl benzoylformate on Pt/Al<sub>2</sub>O<sub>3</sub> using (-)-cinchonidine as a catalyst modifier. Tilted and parallel adsorption modes of the modifier were applied in the model. Multicentered adsorption of the modifier and the reactant was considered. For the latter, the number of required sites was determined by quantum chemical calculations at DFT level. The model

gave a sufficient description of the experimentally observed kinetics including both the effect of hydrogen pressure and the modifier amount.

Transient experiments in a continuous fixed bed reactor were performed to obtain a complete picture of the different phenomena occurring during the hydrogenation. High flow rates led to a faster adsorption of the modifier on the catalyst and then, to a more rapid enantiomeric steady-state. Continuous feeding of the modifier is needed to maintain a steady-state enantiomeric excess. Pretreatment of the catalyst with the modifier gave ee steady state faster than without treatment, retarding however, the reaction rate. The productivity obtained in the batch reactor was higher compared to the continuous one due to the lower influence of mass transfer.

A simple, but reliable preparative pulse method was used to determine the adsorption isotherms of (*R*)- and (*S*)-ethyl mandelate in a post-continuous hydrogenation. A linear model of the adsorption isotherm for the stationary phase was obtained describing the adsorption equilibria very well. The distribution coefficients for (*R*)- and (*S*)-ethyl mandelate were 4.09 and 1.98, respectively.

A multitude of breakthrough curves was measured in the tris-[3,5-dimethylphenyl] carbamoyl cellulose as a solid phase. They were fitted with the axial dispersive flow model with the Linear Driving Force (LDF) approximation incorporated into the software gProms.

In general, a very good agreement between experimental and simulated data was achieved. This proved the reliability of the preparative pulse methodology in providing accurate data on adsorption isotherms of the enantiomers for the investigated adsorbents investigated. Additionally, SMB operating conditions were determined with a simplified model based on the equilibrium theory, i.e., in the absence of mass transfer resistances and hydrodynamic dispersive effects.

A new integrated concept for the production of optically active chemicals by using heterogeneous asymmetric catalysis and chromatographic separation techniques was developed for the synthesis of (*R*)-ethyl mandelate from ethyl benzoylformate. This work has shown that the catalyst, reaction conditions, reactors and separation technology can be integrated to enable a sustainable and economically feasible in a process for the production of optical isomers.

## 5 NOTATION

$C_{0,i}$	Equilibrium liquid phase concentration component $i$
$C$	Concentration of species
$C_0$	Total concentration of active sites
$D_a$	Axial dispersion coefficient
$D_{m,i}$	Molecular diffusivity
$F$	Solid-liquid phase ratio
$f, m, n, p, q$	Number of sites needed for adsorption
$k$	Rate constant
$K$	Equilibrium constant
$K'$	Merged parameter
$Q$	Objective function
$r$	Reaction rate
$t$	Time
$k_{n,i}$	Mass transfer coefficients for the homogeneous particle
$K_i$	Adsorption equilibrium constant of component $i$
$L$	Bed length
$Pe$	Peclet number
$Q$	Volumetric flow rate
$\bar{q}_i$	Average adsorbed solid-phase concentrations of the component $i$
$q_i^*$	Equilibrium solid phase concentration component $i$
$R_p$	Particle radius
$t_R$	Retention time (first statistical moment of peak)
$t_0$	Retention time of unretained tracer
$u_{int}$	Interstitial velocity
$V_C$	Bed volume
$z$	Axial coordinate

### Greek letters

$\alpha$	Selectivity
----------	-------------

$\varepsilon$	Bed bulk porosity
$\varepsilon_p$	Particle porosity
$\sigma^2$	Variance
$\tau_p$	Tortuosity
$\theta$	Fractional coverage
$\rho_B$	Catalyst mass-to-liquid volume (catalyst bulk density)

#### **Abbreviations**

TTBB	1,3,5-Tri-tert-butylbenzene
A	Ethyl benzoylformate
B	( <i>R</i> )-ethyl mandelate
C	( <i>S</i> )-ethyl mandelate
M	Modifier (Cinchonidine)

## 6 REFERENCES

- AB, Eka Chemicals (2007). *Polysaccharide-based chiral HPLC phases for better performance*. Bohus.
- Augustine, R. Warner, R. Melnick, M. (1984). *J. Org. Chem.* , 49, 4853.
- Baldyga, L. M. (2012). *Effect of Platinum Particle Size on the Sulfur Deactivation of Hydrogenation*. University of South Florida.
- Blaser, H.-U. Jalett, H.-P. Wiehl, J. (1991). *J. Mol. Catal.* , 68, 215-222.
- Blöchl., P. E. (1994). *Phys. Rev. B* , 50, 17953-17979.
- Bodmer, M. Mallat, T. Baiker, A. (1998). *Catalysis of Organic Reactions*. (H. F.E, Ed.) New York: Marcel Dekker.
- Bürgi, T. Baiker, A. (1998). *J. Am. Chem. Soc.* , 120, 12920-12926.
- Chemical Engineering News. (2001).
- Enkovaara, J. Rostgaard, C. Mortensen, J. J. Chen, J. Dulak, M. Ferrighi, L. Gavnholt, J. Glinsvad, C. Haikola, V. Hansen, H. A. Kristoffersen, H. H. Kuisma, M. Larsen, A. H. Lehtovaara, L. Ljungberg, M. Lopez-Acevedo, O. Moses, P. G. Ojanen, J. Olsen, T. Petzold, V. Romero, N.A.Stausholm, J. Strange, M. Tritsarlis, G.A. Vanin, M. Walter, M. Hammer, B. Häkkinen, H. Madsen, G.K.H. Nieminen, R.M. Nørskov, J. K. Puska, M. Rantala, T. T. Schiøtz, J. Thygesen K. S. Jacobsen, K.W. (2010). *J. Phys.: Condens. Matter* , 22, 253202-253226.
- Haario, H. (2001). *Modest 6.0-A User's Guide*. Helsinki: ProfMath.
- Hegstrom, R. A. (1990). *Scientific American*. 98.
- Huck, W.-R. Mallat, T. Baiker, A. (2003). *Catal. Lett.* , 87, 241-247.
- Izumi, Y. (1983). *Adv. Catal.* , 32, 215-271.

- Künzle, N. Szabo, A. Wang, Z. Schürch, M. Mallat, T. Baiker, A. (1998). *J. Chem. Soc. Chem. Commun* , 1377-1378.
- Laidler, K. J. (1987). *Chemical Kinetics*. New York: Harper & Row.
- Lieske, H. Lietz, G. Spindler, H. Völter, J. (1983). *J. Catal.* , 81, 8-16.
- Luz, D. A. Rodrigues, A. K. O. Silva, F. R. C. Torres, A. E. B. Cavalcante Jr. C. L. Brito, E. S. Azevedo. D. C. S. (2008). *Biores. Tech.* , 99, 2455-2465.
- Mallat, T. Bodmer, M. Baiker, A. (1997). *Catal. Lett.* , 44, 95-99.
- Martin, G. Mäki-Arvela, P. Murzin. D. Yu. Salmi, T. (2013). *Cat. Lett.* , 143, 1051-1060.
- Orito, Y. Imai, S. Niwa, S. (1979). *Nippon Kagaku Kaishi* , 1118-1120.
- Pasteur, L. (1848). *C. R. Acad. Sci.* , 26, 535-545.
- Pereira, C.S.M. Zabka, M. Silva, V.M.T.M. Rodrigues, A.E. (2009). *Chem. Eng. Sci.* , 64, 3301-3310.
- Rabelo, M.C. Pereira, C.S.M. Rodrigues, S. Rodrigues, A. E. Azevedo, D. C. S. (2013). *Ads. Sci. Tech.* , 30, 773-784.
- Ruiz, D. Reyes, P. (2008). *J. Chil. Chem. Soc.* , 53, 1740-1742.
- Schürch, M. Künzle, N. Mallat, T. Baiker, A. (1998). *J. Catal.* , 176, 569-571.
- Schürch, M. Schwalm, O. Mallat, T. Weber, J. Baiker, A. (1997). *J. Catal.* , 169, 275-286.
- Sexton, B. A. Hughes, A. E. (1984). *Surf. Sci.* , 140, 227-234.
- Sheldon, R. A. (1993). *Chitotechnology: Industrial synthesis of optically active compounds*. New York: Marcel Dekker.
- Studer, M. Burkhardt, S. Blaser, H.-U. (1999). *Chem. Commun.* 1727-1730.
- Sunjic, V. (2009), *Croat. Chem. Acta*, 82, 503-530.
- Sutherland, M. Ibbotson, A. Moyes, R. B. Well, P. B. (1990). *J. Catal.* , 125, 77-88.

- Tokarev, A.V. Kirilin, A.V. Murzina, E.V. Eränen, K. Kustov, L.M. Murzin, D.Yu. Mikkola. J. 2010. (2010). *Int. J. Hydrogen Energy* , 35, 12642-12649.
- Toukoniitty, E. Mäki-Arvela. P. Kuusisto, J. Nieminen, V. Päivärinta, J. Hotokka, M. Salmi, T. Murzin, D. Yu. (2003). *Journal of Molecular Catalysis A: Chemical* , 192, 135-142.
- Toukoniitty, E. Mäki-Arvela, P. Kumar, N. Salmi, T. Murzin, D. Yu. (2003). *Catalysis Today* , 79, 189-193.
- Toukoniitty, E. Wärnå, J. Murzin, D.Yu. Salmi, T. (2010). *Chem. Eng. Sci.* , 65, 1076-1087.
- von Arx, M. Mallat, T. Baiker, A. (2000). *J. Catal.* , 193, 161-164.
- Wang, G.Z. Mallat, T. Baiker, A. (1997). *Tetrahedron: Asymetry* , 8, 2113-2140.
- Weissermel, K. L. Arpe, H. (1997) *Industrial Organic Chemistry*. 3<sup>rd</sup>. New York: VCH Publishers Inc.
- Wellendorff, J. Lundgaard, K.T. Møgelhøj, A. Petzold, V. Landis, D.D. Nørskov, J. K. Bligaard T. Jacobsen K. W. (2012). *Phys. Rev. B.* , 85, 235149-235172.



ISBN 978-952-12-3072-1  
Painosalama Oy – Turku, Finland 2014